BUREAU OF RECLAMATION

Seepage Detection and Characterization in a Truckee Canal Site using L-band Synthetic-Aperture Radar (SAR) Technology

Science and Technology Program
Research and Development Office
Final Report No. ST-2021-19258-01

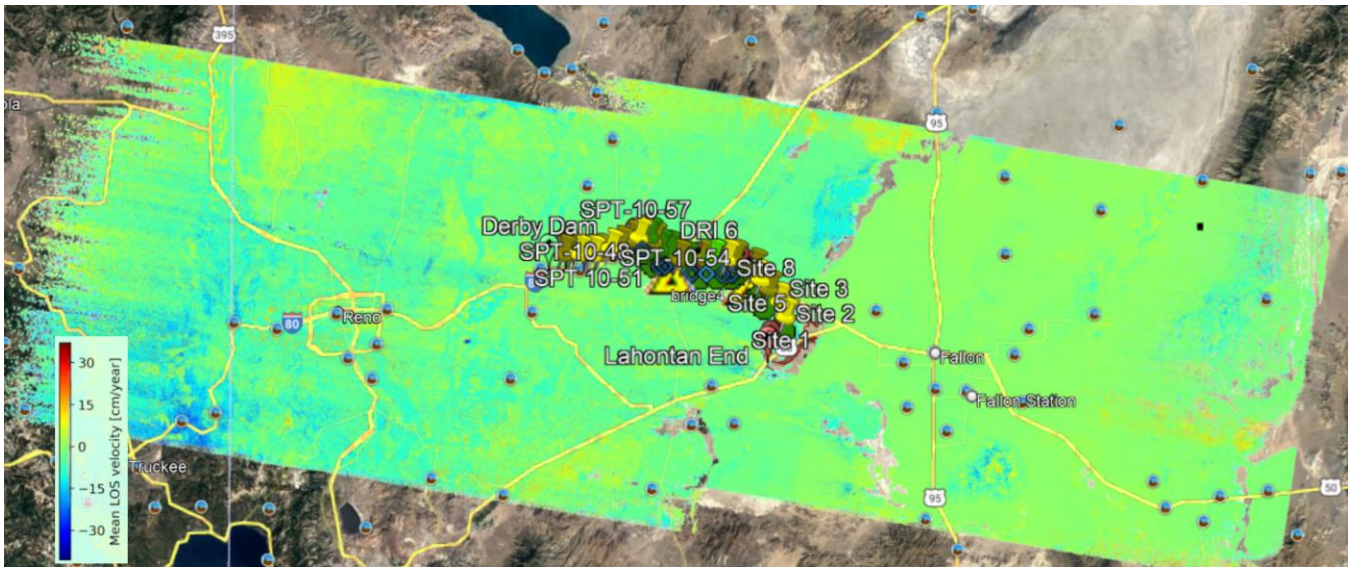

U.S. Department of the Interior September 2021

REPORT DOCUMENTATION PAGE

Form Approved
OMB No. 0704-0188

PLEASE DO NOT RETURN YOUR FORM TO THE ABOVE ADDRESS.

1. REPORT DATE *(DD-MM-YYYY)*	**2. REPORT TYPE**	**3. DATES COVERED** *(From - To)*
9/30/2021	Research	FY18 to FY21

4. TITLE AND SUBTITLE
Seepage Detection and Characterization in a Truckee Canal Site using L-band Synthetic-Aperture Radar (SAR) Technology

5a. CONTRACT NUMBER
RR4888FARD1902201 / F013A

5b. GRANT NUMBER

5c. PROGRAM ELEMENT NUMBER
19258 (S&T)

6. AUTHOR(S)
Jong Beom Kang, BOR, Civil Engineer

5d. PROJECT NUMBER
Final Report ST-2021-19258-01

5e. TASK NUMBER

5f. WORK UNIT NUMBER

7. PERFORMING ORGANIZATION NAME(S) AND ADDRESS(ES)
Bureau of Reclamation, Technical Service Center, Denver Federal Center, Denver, CO

8. PERFORMING ORGANIZATION REPORT NUMBER

9. SPONSORING/MONITORING AGENCY NAME(S) AND ADDRESS(ES)
Science and Technology Program
Research and Development Office
Bureau of Reclamation
U.S. Department of the Interior
Denver Federal Center
PO Box 25007, Denver, CO 80225-0007

10. SPONSOR/MONITOR'S ACRONYM(S)
Reclamation

11. SPONSOR/MONITOR'S REPORT NUMBER(S)
Final Report ST-2021-19258-01

12. DISTRIBUTION/AVAILABILITY STATEMENT
Final Report may be downloaded from https://www.usbr.gov/research/projects/index.html

13. SUPPLEMENTARY NOTES

14. ABSTRACT
This research is aimed at evaluating the SAR satellite remote sensing technology to identify potential seepage locations for more rapid and global management of canals.

15. SUBJECT TERMS
Canals, Seepage detection, SAR, Satellite remote sensing

16. SECURITY CLASSIFICATION OF:			**17. LIMITATION OF ABSTRACT**	**18. NUMBER OF PAGES**	**19a. NAME OF RESPONSIBLE PERSON**
a. REPORT	**b. ABSTRACT**	**THIS PAGE**			Jong Beom Kang
U	U	U		35 Pages	**19b. TELEPHONE NUMBER** *(Include area code)* 303-445-2375

Mission Statements

The Department of the Interior (DOI) conserves and manages the Nation's natural resources and cultural heritage for the benefit and enjoyment of the American people, provides scientific and other information about natural resources and natural hazards to address societal challenges and create opportunities for the American people, and honors the Nation's trust responsibilities or special commitments to American Indians, Alaska Natives, and affiliated island communities to help them prosper.

The mission of the Bureau of Reclamation is to manage, develop, and protect water and related resources in an environmentally and economically sound manner in the interest of the American public.

Disclaimer

Information in this report may not be used for advertising or promotional purposes. The data and findings should not be construed as an endorsement of any product or firm by the Bureau of Reclamation, Department of Interior, or Federal Government. The products evaluated in the report were evaluated for purposes specific to the Bureau of Reclamation mission. Reclamation gives no warranties or guarantees, expressed or implied, for the products evaluated in this report, including merchantability or fitness for a particular purpose.

Acknowledgements

The Science and Technology Program, Bureau of Reclamation, sponsored this research.

Seepage Detection and Characterization in a Truckee Canal Site using L-band Synthetic-Aperture Radar (SAR) Technology

Final Report No. ST-2021-19258-01

prepared by

Bureau of Reclamation
Technical Service Center
Jong Beom Kang, TSC, Civil Engineer

Peer Review

Bureau of Reclamation
Research and Development Office
Science and Technology Program

Final Report No. ST-2021-19258-01

Seepage Detection and Characterization in a Truckee Canal Site using L-band Synthetic-Aperture Radar (SAR) Technology

JONG BEOM KANG

Digitally signed by JONG BEOM KANG
Date: 2021.09.30 11:15:15 -06'00'

Prepared by: Jong Beom Kang
Civil Engineer, Geotechnical Laboratory and Field Support, 86-68550

Peer Review: Scott Baker
InSAR Specialist, BOS Technologies

"This information is distributed solely for the purpose of pre-dissemination peer review under applicable information quality guidelines. It has not been formally disseminated by the Bureau of Reclamation. It does not represent and should not be construed to represent Reclamation's determination or policy."

Contents

Tables

Figures

Executive Summary

Reclamation alone holds 8,116 miles of in-service water conveyance canals within its infrastructure inventory. Many of these canal systems have aged beyond their original intended lifespan and are showing signs of aging and disrepair, extensive seepage and embankment failure events are becoming increasingly common, and consequences of canal failures within urban corridors are constantly increasing due to urban encroachment on these water conveyance structures. In addition to the problem of increased risk related to canal embankment failures, concentrated and distributed seepage poses a major challenge to water conservation due to significant water conveyance system losses.

As a result, there is an ongoing need to identify and comprehensively characterize canal seepage, both for safety-related and water conservation efforts and is the main motivation for this proposed research. The seepage detection and characterization in canal sites by means of the Synthetic-Aperture Radar (SAR) satellite remote sensing technology is an important research topic to evaluate suitable resolution and realistic limitations of the SAR to detect canal seepage and be used as a comprehensive monitoring technique for identification of potential seep locations at canal infrastructure.

SAR data processing platforms for identification of potential seep locations at canals are reviewed, summarized, and selected for this research. The InSAR Scientific Computing Environment (ISCE) designed for the purpose of processing Interferometric Synthetic Aperture Radar (InSAR) data was chosen to perform timeseries analysis to identify known seepage locations in Truckee Canal.

In this research, C-band Sentinel-1A and -1B satellite imagery data with historical 6- or 12-day repeat cycles are collected to cover the Truckee Canal project site and the timeseries analysis to identify potential seepage locations was performed. L-band Advanced Land Observing Satellite (ALOS) imagery data was not used for timeseries analysis because historical ALOS satellite imagery acquisitions were planned with 46-day repeat cycles that does not offer a sufficient temporal resolution to capture time-lapse responses following operation events or standing water events in summer.

The InSAR data processing results at known seep locations indicate that corresponding dates of canal watering-up/de-watering correlate with the changes of SAR mean line-of-sight (LOS) velocity (mm/year) values obtain from timeseries analysis at known seep locations.

C-band radar operating system at shorter wavelengths than L-band are more sensitive to sparse and low biomass vegetation. Therefore, L-band and P-band will be suitable Satellite frequency bands with high resolutions to detect seepage other than C-band Satellite imagery data. Although P-band is most preferred for seepage detection, its use is limited to airborne deployments using airborne Uninhabited Aerial Vehicle Synthetic Aperture Radar (UAVSAR). Water seepage through the canal prism into the subsurface soil layers is a major water conveyance loss in irrigation canal systems. If the canal seepage is monitored and detected by using the InSAR monitoring technology with proper satellite frequency bands, canal prism and embankments can be properly maintained in the long-term canal infrastructure performance.

1. Background

Water resources are conveyed by canal infrastructure systems to water users. Water loss along irrigation canals is inevitable due to evaporation and transpiration in the water cycle. However, the major water conveyance loss in irrigation canal systems is seepage water through the canal prism into the subsurface soil layers. Seepage that is not properly detected and repaired can result in a potential canal prism failure in the long-term canal infrastructure performance. A more effective water conveyance system for water resources is critical as population increases and climate change influences drought years.

Synthetic Aperture Radar (SAR) satellite remote sensing technology has been broadly applied to various fields and produced an extraordinary range of applications including agriculture, disaster monitoring and mitigation, water resource management, environmental monitoring, mineral exploration, land use mapping, and coastal eco-system monitoring (Lievens et al., 2011; Leroux et al., 2016; Magagi et al., 2013; Das et al., 2001, 2014; Kim et al., 2017a; 2017b; 2016a; 2016b; 2014; 2012; 2011; 2010). SAR technology application is growing rapidly and has significantly contributed on several areas with varying spatial resolutions.

SAR satellite remote sensed imagery data have become an important tool to obtain earth image data by measuring electromagnetic radiation reflected from surface and subsurface materials. Satellites with SAR sensors can cover much larger areas and are highly effective in damage surveys since SAR can be used regardless of sunlight and weather conditions. For example, a significant event, the Kobe earthquake areas with heavy damage and liquefaction were identified and observed by using SAR satellite imagery data (Yamazaki, 2003).

The InSAR technique could lead to the ability for Reclamation to 1) quickly and effectively identify previously unknown seepage areas on a system-wide or even nation-wide scale, 2) monitor known seepage areas for disconcerting changes, 3) help in identifying priority sections for focused maintenance efforts, 4) differentiate between suspected seepage and natural groundwater drainage phenomena not related to canal water losses, 5) evaluate canal liner performance based on pre/post installation seepage levels, 6) evaluate canal damage repair and other proactive maintenance activities (e.g., berm installations) based on pre/post seepage conditions, 7) identify changes in seepage following standard canal dredging activities, which have occasionally been suspected of initiating or exacerbating seepage losses, 8) identify other structures/areas/phenomena that could be better characterized using this technology

The InSAR technique will provide enhanced seepage detection and characterization approaches to the Reclamation area offices and other agencies, directly help Reclamation manage water resources efficiently, and potentially be applicable to other earthen embankment sites and structures in order to identify and prioritize potential repair locations to promote healthy water conveyance and storage infrastructure. These periodically collected SAR data and the time-series analysis results will provide valuable information within a short time period to detect any potential risks.

2. Scope of Research

For the proof-of-concept research effort of the InSAR technique to provide enhanced seepage detection and characterization approaches in canals, the following tasks were performed: (1) getting known seep location data from the Lahontan Basin Area Office (LBAO) in the Truckee Canal, (2) providing prioritized known seep location data for the InSAR data processing, (3) Collecting historical 46-day and 6- or 12-day repeat imagery data from ALOS and Sentinel satellites at study areas, (4) installing piezometer and observation wells perpendicular to some of the known seepage locations, (5) performing slug tests to estimate hydraulic conductivity values of subsurface soils at selected known seep locations along the canal, (6) developing and calibrating seepage models, (7) conducting InSAR timeseries analyses to evaluate whether the SAR approach is feasible for detecting seepage locations throughout the Truckee Canal test-site, and (8) finalizing a summary report of findings of this research effort.

The strategy of this research study consists of the following general task descriptions:

Task1: Obtain the following existing known seep data from the Lahontan Basin Area Office (LBAO) along the Truckee Canal in Nevada: (1) seep locations (e.g., x and y coordinates), (2) when the seep happened (e.g., date and time), (3) when the seep was repaired with maintenance periods (e.g., date and time for any repairs or maintenance), (4) when the canal was watering-up/de-watering annually (e.g., time period of March through November), (5) channel water levels at known seep locations for a boundary condition, and (6) observation well response (x, y coordinates and reading data) near known or unknown seep locations during the seepage losses.

Task2: Provide prioritized known seep location data to initiate a feasibility level of proof-of-concept efforts for the SAR seepage detection approach. LBAO has more than 40 seeps mapped in GIS and a number of seeps that have been repaired since 2015; these known seep locations should be prioritized for the SAR seepage detection application. Corresponding annual dates of canal watering-up and de-watering will help focus the SAR Technology data locations and times of interest for the initial proof-of-concept effort.

Task3: Collect historical 46-day and 6- or 12-day repeat imagery data from ALOS and Sentinel satellites at study areas to cover the mountains of Sierra Nevada between the Central Valley of California and the Great Basin and San Juan Mountains in the Rocky Mountains in southwestern Colorado and northwestern New Mexico.

Task 4: Install piezometer and observation wells perpendicular to the canal at some of the known seepage locations to calibrate the seepage models. The hydraulic head data measured from the piezometer/observation wells will be useful to ground truth points for validating the SAR data and tuning initial seepage models to estimate seepage rates and hydraulic conductivity values of subsurface soils.

Task 5: perform slug tests to estimate hydraulic conductivity values of subsurface soils at selected known seep locations along the canal,

Task 6: Develop and calibrate energy transport and hydraulic models. The seepage models will include geological profiles for the entire study site and be calibrated with hydraulic conductivities quantified from slug tests.

Task 7: Perform timeseries analyses of SAR data with the following analyses: 1) identify the spatial changes in SAR image data that likely correlate with known seepage targets, and 2) conduct time lapse analyses based on the coordinates of known seeps and corresponding dates of canal operations

Task 8: Evaluate the need for the continuation of research and the extension/application of the effort to additional canal systems/sites throughout the US, contingent on the results and success of this initial proof-of-concept research effort.

Task 9: Finalize a summary report of findings from this research effort. The findings of this study will be reviewed by interested regional partners and TSC researchers. All the findings will be included in a report.

3. Previous Work

Synthetic Aperture Radar (SAR) satellite remote sensing technology has been broadly applied to various fields and produced an extraordinary range of applications including agriculture, disaster monitoring and mitigation, water resource management, environmental monitoring, mineral exploration, land use mapping, and coastal eco-system monitoring (Lievens et al., 2011; Leroux et al., 2016; Magagi et al., 2013; Das et al., 2001, 2014; Kim et al., 2017a; 2017b; 2016a; 2016b; 2014; 2012; 2011; 2010). SAR technology application is growing rapidly and has significantly contributed on several areas with varying spatial resolutions. The spatial resolution is categorized as low (30m or more), medium (5m to 30m), high (1m to 5m), or very high (1m or less).

L-band SAR sensor is an easy approach to process and implement due to its relatively lower frequencies (e.g., 1 to 2 GHz), less expensive equipment, and wider beam width with a return interval of 6 days and multi-polarization. L-band SAR satellite remote sensing technology can be used to detect and quantify potential seepage losses for more rapid and global management at canal embankments.

The time-lag analyses result from the SAR responses could be validated in comparing to volumetric water content (VWC) obtained from the field or laboratory test data. The VWC is a vital parameter in water resource management in the agricultural and ecological fields. There are several methods used to estimate VWCs. Equipment for direct soil water content measurements varies and is available from many manufacturers (IAEA, 2008). A neutron probe device is calibrated for in situ conditions at various depths. The correlation between the measured gravimetric soil water content and neutron probe ratio is relatively high and volumetric water contents are estimated from gravimetric water contents (Jabro et al., 2005).

The SAR satellites data has been widely used in (1) water-related applications such as snow depth estimation, river channel mapping, soil moisture retrieval, and aquifer volume changes, and (2) deformation-related applications such as volcano monitoring, earthquake damage mapping, ice stream motion, landslide monitoring, and land subsidence due to sink holes and waste-water disposal

activities. The C- and L-band SAR remote sensing technology can assist in identifying seepage locations or channel planform changes at canal, river, and levee structures.

A primary benefit of this technology is that, in most cases, a significant amount of historical data exists which can be used to "hind-cast" previous performance. These data can then be used to inform locations and techniques for more detailed investigations or can be used to constrain models.

Satellite-based radar has better capability than optical/thermal infrared in detecting wetness under vegetation and topsoil. There are three key practical considerations necessary to monitor canal seepage remotely: spatial resolution, temporal resolution, and spatial coverage. The SAR data at 10- m spatial resolution estimates surface volumetric water content (VWC) of soil near canals allowing for estimates of canal seepage that can be compared with field/lab test results. However, speckling noise from backscattering of thermal, vegetation, and surface roughness might cause challenges in mitigating potential errors in the SAR data. There are multiple possible causes of the missed detection, including rain events that may cause speckling noise or a radar signal associated with wetting may be too small. Reduction of the missed detections will be investigated in the future using the following approaches: 1) multi-temporal despeckling method, which has not been implemented, may reduce the noise, 2) a spatial feature enhancement by the nonlocal mean filter, 3) systematically removing the vegetation effect using the physical model approach that worked effectively for soil moisture studies, 4) examining the longer wavelength observation to identify subsurface seepage such as L-band ALOS satellite data or NASA's L- or P-airborne data, 5) using the approaches for the Soil Moisture Active Passive mission (SMAP) to derive soil moisture which could provide more detailed information of wetting due to seepage, and 6) spatially multi-looking the ground range detected (GRD) data product to reduce speckle noise and Sentinel Application Platform (SNAP) satellite software provided by European Space Agency (ESA).

The upcoming NASA-ISRO SAR (NISAR) is planning on launching a dual-frequency synthetic aperture radar in September 2022 that is expected to have advanced radar imaging to observe and understand natural processes on ground surface. Our goal is to utilize the radar ability to detect under vegetation and topsoil with frequent monitoring over a continental scale and apply it towards operational monitoring of canal leaks and implement more sophisticated algorithms that have been used widely in the SAR community.

The L-band SAR can provide more detailed analysis of canal seepage by: 1) cataloging the spatial variations in SAR satellite images related to shallow (≤5 cm below ground surface) soil moisture distributions, 2) conducting time-lapse analyses for temporal change detection on a per-satellite-image-pixel basis, and 3) identifying spatio-temporal changes following operations and maintenance events along canals (e.g., watering-up of a canal system, or pre/post embankment lining or repair efforts), in order to help evaluate changes in performance and hydrologic conditions along the embankment.

This seepage detection approach using the C- and L-band SAR satellite remote sensing technology provides a technique to quantify potential seepage losses by location and over time, for more rapid and global management of canal embankments.

The SAR data processing consists of five major steps: (1) SAR data collection, (2) data pre-processing, (3) interferogram generation, (4) phase unwrapping, and (5) geocoding.

Step 1. In SAR data collection, multiple-year L-band and C-band satellite image data archived from the ALOS-1(L-band) and Sentinel-1A/B (C-band) can be searched, accessed, and collected from SSARA (Seamless SAR Archive). https://web- services.unavco.org/brokered/ssara/gui.
Step 2. In the pre-processing step, orbit data are used to compute offset vectors on pixel level from Single Look Complex (SLC) images. The processed image is resampled to the master grid. Co-registered stacks of single-look complex (SLC) data can be created to generate surface displacement time-series followed by further analysis of the phase and amplitude.
Step 3. In the interferogram generation, interferometric products are computed to generate the complex interferogram and the coherence images. The interferometric phase can be corrected for the phase of a ground control reference point and coherence changes can be compared through time.
Step 4. In the phase unwrapping step, original phase from the wrapped phase representation is reconstructed with a sophisticated phase unwrapping algorithm.
Step 5. In the geocoding, the unwrapped phase is converted to a height and the pixel coordinates are georeferenced. The generated products can be modified for contouring and layering with GIS programs.

SAR satellite remote sensing technology using 10-m full resolution and 30-m multi-looked data can be used to detect soil moisture content and time-lapse fluctuations in concentrated and distributed seepage. Historical and recent SAR satellite imagery from multiple missions and international space agencies are available to download for free. Multiple-year L-band and C-band SAR data archived from the ALOS-1(L-band, 46-day repeat, 2006-2011) and Sentinel-1A/B (C-band, 6- and 12-day repeat, 2015- present) satellites are readily available with more L-band data available in the future from ALOS-2 (2014-present) and NISAR (launching in 2022). Future radar missions, such as NASA-ISRO SAR (NISAR) operating at L-band are expected to have improved Radar Frequency Interference (RFI) and geolocation. SAR satellite remote sensing technology aids in effective detection of seepage loss areas on a wide scale allowing for a rapid evaluation/monitoring of canal embankment systems, and efficient cost saving to cover nationwide canal sites.

4. SAR Processing Platform

The following SAR data processing platforms are described within this section: (1) Google Earth Engine (GEE), (2) SNAP (Sentinel Application Platform), and (3) ISCE/MintPy.

4.1 Google Earth Engine

Google introduced Google Earth Engine (GEE) to enhance the applications of satellite imagery for large scale applications in the 2010s. GEE is a web-based platform providing global-scale geospatial analysis with preprocessed Sentinel-1 backscatter images and the cloud computing infrastructure (Gorelick, et. al., 2017).
The GEE cloud-based platform provides new options for researchers interested in geospatial data analysis as providing machine learning algorithms and massive computational capabilities of remote sensing data on various societal issues including drought, water management, disaster, disease, and climate monitoring.

The advantage of the GEE cloud-based platform is its computational speed as utilizing Google's servers. The GEE platform provides constantly updated datasets and the datasets can be accessed within the code editor (https://code.earthengine.google.com).

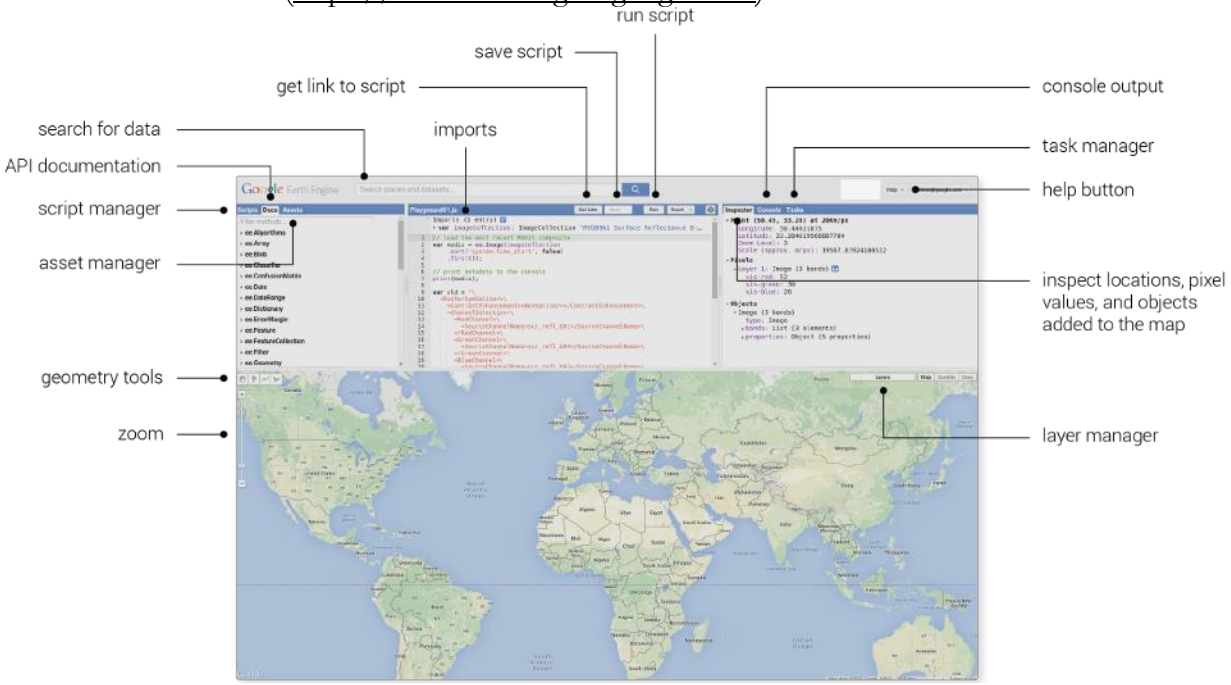

Figure 1. Earth Engine Code Editor with a web-based Integrated Development Environment (IDE) for the Earth Engine JavaScript Application Programming Interfaces (APIs).

The simplified procedure how to visualize different composites in Google Earth Engine is as follows.

Step 1. Preparation framework

The framework to prepare Sentinel-1 SAR backscatter Analysis Ready Data (ARD) is briefly described in Figure 15. The framework includes additional border noise correction, speckle filtering, and radiometric terrain normalization and can be applied to a Sentinel-1 GEE image collection. The additional preprocessing is optional and can be revised on application needs and specific requirements for the analysis. The framework is initiated in both the Python application programming interface (API) and GEE Java script (Mullissa et al. 2021).

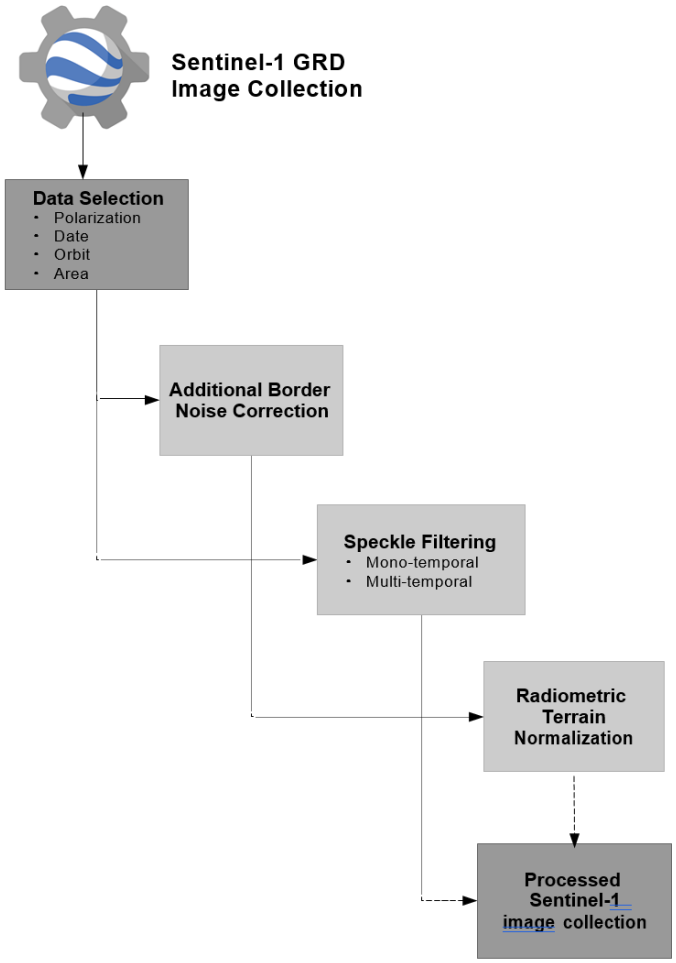

Figure 2. Preparation framework to create Sentinel-1 ARD in GEE. The dark and light grey boxes depict mandatory and optional preprocessing steps, respectively (Mullissa et al. 2021).

Step 2. Specify an area of interest and Sentinel-1 data selection

Selection of the location of the study area is necessary to specify the processing extent of the geospatial analysis and avoid redundant computations.

Sentinel-1 imagery data collection in GEE includes Sentinel-1 Ground Range Detected (GRD) scenes that are processed as using the Sentinel-1 Toolbox to generate a calibrated and ortho-corrected product.

The daily updated data collection includes all Sentinel 1-A and 1-B GRD image products acquired in both ascending and descending orbits in interferometric wideswath (IW) mode. The Sentinel-1 GRD images have a pixel spacing of 10 m at which the full information detail is guaranteed, and a spatial resolution

Sentinel-1 satellites provide temporally dense and high spatial resolution synthetic aperture radar (SAR) imagery and acquires images globally every 6 to 12 days. Sentinel-1 GRD data in the GEE catalogue can be collected as all the preprocessing steps require the data to be in linear scale. Sentinel-1 imagery in single polarization (i.e., VH or VV) or dual polarization mode (i.e., VV and VH) can be considered (Di Martino et.al., 2013).

Step 3. Time frame & sensor parameters selection

The user is required to setup time frame of pre- and post-event periods and Sentinel-1 imagery is acquired a minimum of every 12 days for each point globally. Sentinel-1 has different polarization options that "VV" means vertically polarized signal transmitted out and vertically polarized signal received, whereas VH refers to vertically polarized signal transmitted out, and horizontally polarized signal is received.

VV: single co-polarization, vertical transmit/vertical receive
HH: single co-polarization, horizontal transmit/horizontal receive
VV + VH: dual-band cross-polarization, vertical transmit/horizontal receive
HH + HV: dual-band cross-polarization, horizontal transmit/vertical receive

User also can select between 'VH' and 'VV' polarization to perform the analysis. 'VH' is widely used, since it is more sensitive to changes on the land surface, while 'VV' is rather susceptible to vertical structures and might be useful to delineate open water from land surface (e.g. a large water body).
User might choose between 'DESCENDING' and 'ASCENDING' pass direction, depending on the study area. It is necessary to select the same pass direction for the images being compared to avoid false positive signals caused by differences of the viewing angle when performing change detection.

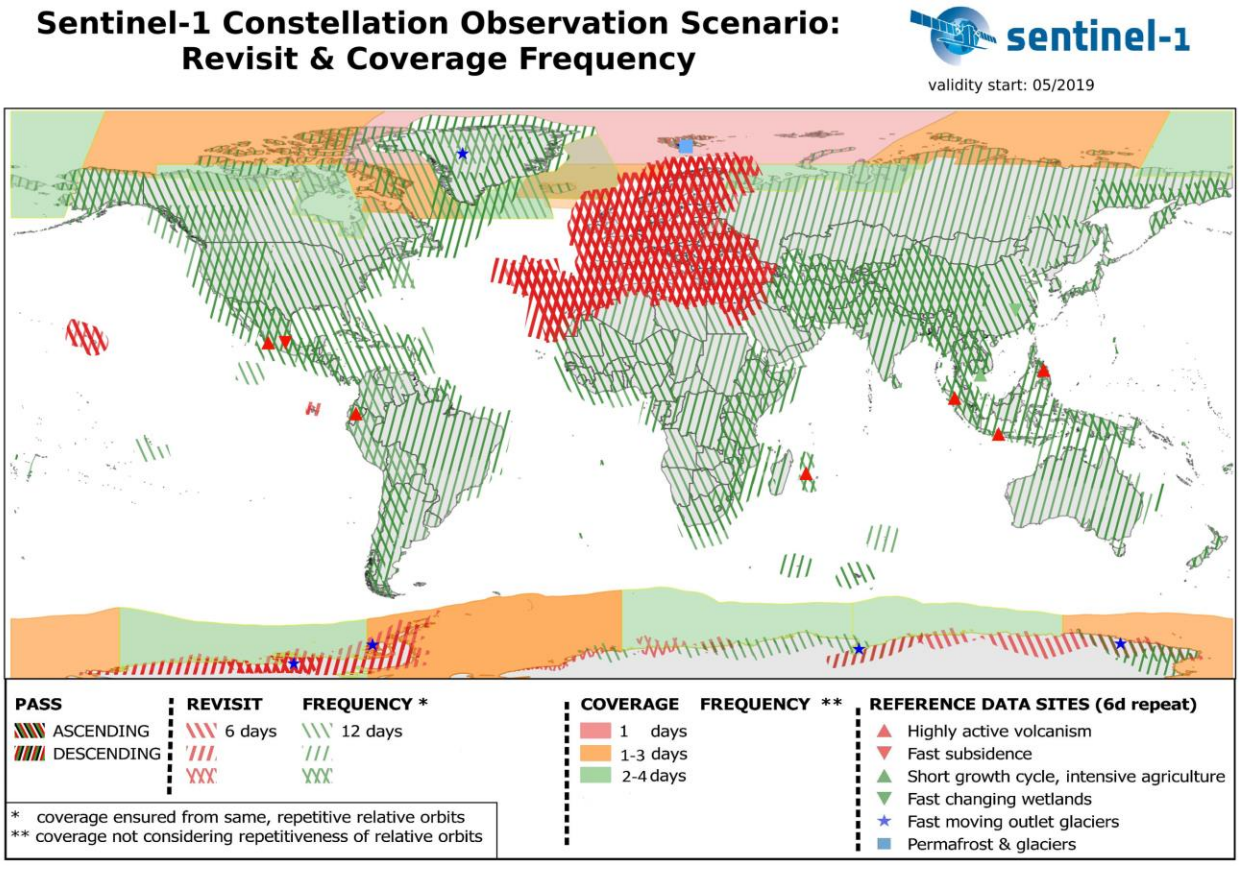

Figure 3. Revisit and coverage frequency of the Sentinel-1 constellation, showing which areas are mainly covered with descending or ascending imagery. Source: https://sentinel.esa.int/web/sentinel/missions/sentinel-1/observation-scenario

Entire Sentinel-1 GRD archive in Google Earth Engine is filtered by the instrument mode, the polarization, pass direction, and spatial resolution at the boundary of the area of interest.

Step 4. Preprocessing
Information from Sentinel-1 Level-1 Ground Range Detected (GRD) imagery in Google Earth Engine has already undergone the following preprocessing steps: (1) Apply-orbit-file (updates orbit metadata), (2) ARD border noise removal (removes low intensity noise and invalid data on the scene edges), (3) Thermal noise removal (removes additive noise in sub-swaths), (4) Radiometric calibration (computes backscatter intensity using sensor calibration parameters), (5) Terrain-correction (orthorectification), (6) Conversion of the backscatter coefficient ($\sigma°$) into decibels (dB).
Border noise artifacts were produced when transforming the raw data to level-1 products by the Sentinel-1 Instrument Processing Facility software (IPF). The presence of border noise in Sentinel-1 GRD products is one of the unwanted artifacts that should be removed before further analysis.

Speckle filtering is an important component of SAR image preprocessing as all SAR images are inherently affected by speckle. Users can evaluate the performance of speckle filters qualitatively by visually checking the speckle reduction in homogeneous regions and the preservation of subtle features, such as roads and point scatterers, in the filtered images or quantitatively using the equivalent number of looks (ENL) or coefficient of variation in homogeneous regions in the image.
Radiometric terrain normalization is important to mitigate the effect of topography on the SAR backscatter. Angular between the SAR image and the terrain geometry based radiometric terrain normalization implemented in GEE depends only on angles, from which a simplified relation between the image and terrain can be derived.
The implementation of speckle filters and radiometric terrain normalization in GEE gives the user options to use different parameters for preprocessing the Sentinel-1 images depending on the envisioned application and scale of processing.
The processing steps are performed automatically when running the Google Earth Engine script. It is useful to understand how the data is being processed, which datasets are used, and what limitations the analysis may have for each case.

Step 5. Visualize results in GEE and export products
When all parameters are selected, run the script and visualize results in GEE. The layers that the user is interested in can be checked or unchecked and a screenshot of the map can be taken as an overview.
To export the generated products into a Google Drive account, click on 'Tasks' in the top-right corner of the code editor and hit 'RUN', and choose where to save the file.
The processed Sentinel-1 ARD image collection can be formatted to a linear power or dB scale. In the absence of radiometric terrain normalization, the data is processed in sigma naught (σ_0). To export the processed image collection, provided are the export-to-asset option so that every image in the collection can be exported to a GEE asset. To aid in visualization and interpretation, the output data format can be changed to a dB scale by the user.

4.2 Sentinel Application Platform (SNAP)

Sentinel Application Platform (SNAP) is a common architecture for all Sentinel Toolboxes, which is useful for earth observation processing and analysis. It is a software with incorporated utilities for interferogram generation and stacking.

Interferometric synthetic aperture radar (InSAR) processing exploits the phase signal difference between two complex radar SAR acquisitions/observations taken from slightly different sensor positions to extract information and analyze the shape and deformation of the earth's surface or objectives.

SAR is an active microwave imaging system obtained from active sensors to detect reflected responses from objectives irradiated by artificially generated energy sources.

The basic measurement from SAR signals includes amplitude and phase information of the complex image. The amplitude is the strength of the radar response of radio-frequency electromagnetic signal reflected from a target and the phase is the fraction of a single and multi-looked radar wavelength.

The Sentinel-1A and Sentinel-1B European radar imaging satellites launched on April 3, 2014 and April 25, 2016, respectively carries C-band SAR sensors, and delivers repeated many SAR acquisitions. InSAR technique, a remote sensing technique, using two or multiple SAR phase images performs time-series analysis to monitor ground deformation changes with many SAR acquisitions

The Sentinel-1 Toolbox (S1TBX) is being developed for European Space Agency (ESA) and called the Sentinel Application Platform (SNAP). The Sentinel-1 Toolbox (S1TBX) consists of (1) a collection of processing tools, (2) data product readers and writers and (3) a display and analysis application to support the large archive of data from European Space Agency (ESA) SAR missions. The Sentinel-1 Toolbox (S1TBX) includes various processing tools for calibration, speckle filtering, co-registration, orthorectification, mosaicking, data conversion, polarimetry and interferometry. The SNAP processing tools for earth observation and analysis could be run independently from the command-line as well as integrated within the graphical user interface. The common features of the SNAP tools include the followings: (1) very fast image display and navigation of giga-pixel images, (2) Graph Processing Framework (GPF) for creating user-defined processing chains, (3) advanced layer management allows adding and manipulation of new, (4) flexible band arithmetic using arbitrary mathematical expressions, (5) accurate reprojection and ortho-rectification to common map projections, (6) geo-coding and rectification using ground control points, (7) multi-threading and multi-core processor support, and (8) graph processing framework.

The steps for InSAR processing with a SNAP (Sentinel Application Platform) are as follows.

Step 1: Open raw data
Open raw data of the zipped Sentinel-1A or -1B Interferometric Wide (IW) Single Look Complex (SLC) or Ground Range Detected (GRD) products.

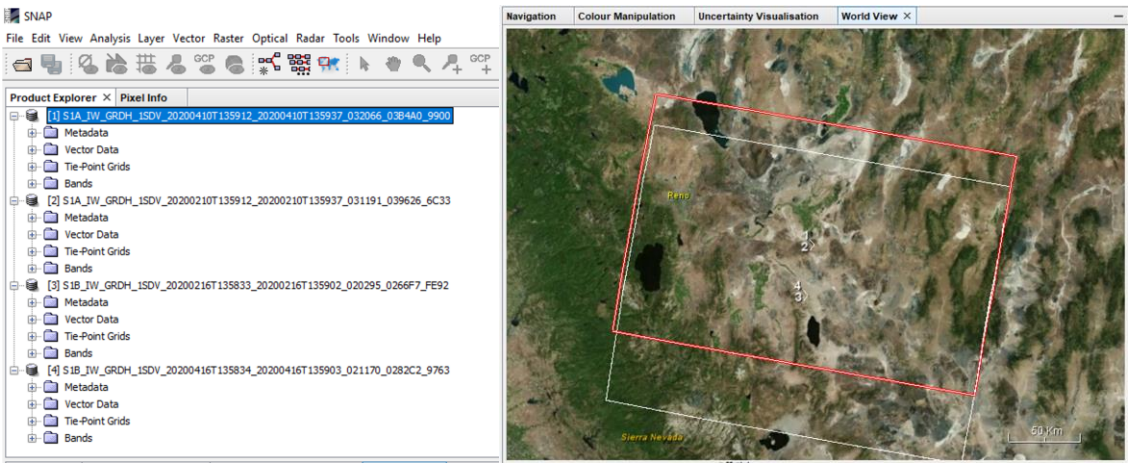

Figure 4. Product explorer and a base map

Step 2: View the products

Each Sentinel-1A or -1B product consists of metadata, vector data, tie-point grids, and bands. The bands contain the actual raster data, organized by polarization and sub-swaths of S1 IW products. The virtual intensity band is to assist in visualizing the complex data.

SAR images include the intensity of radar reflections from ground. The more reflection we have, the brighter the image. The intensity of radar reflections from ground is a measure of moisture and roughness in order to get soil moisture and roughness maps. A SAR image is very dark if we have low backscatter, and it is very bright if we have severe backscatter. Therefore, the brighter image indicates that something has changed on ground.

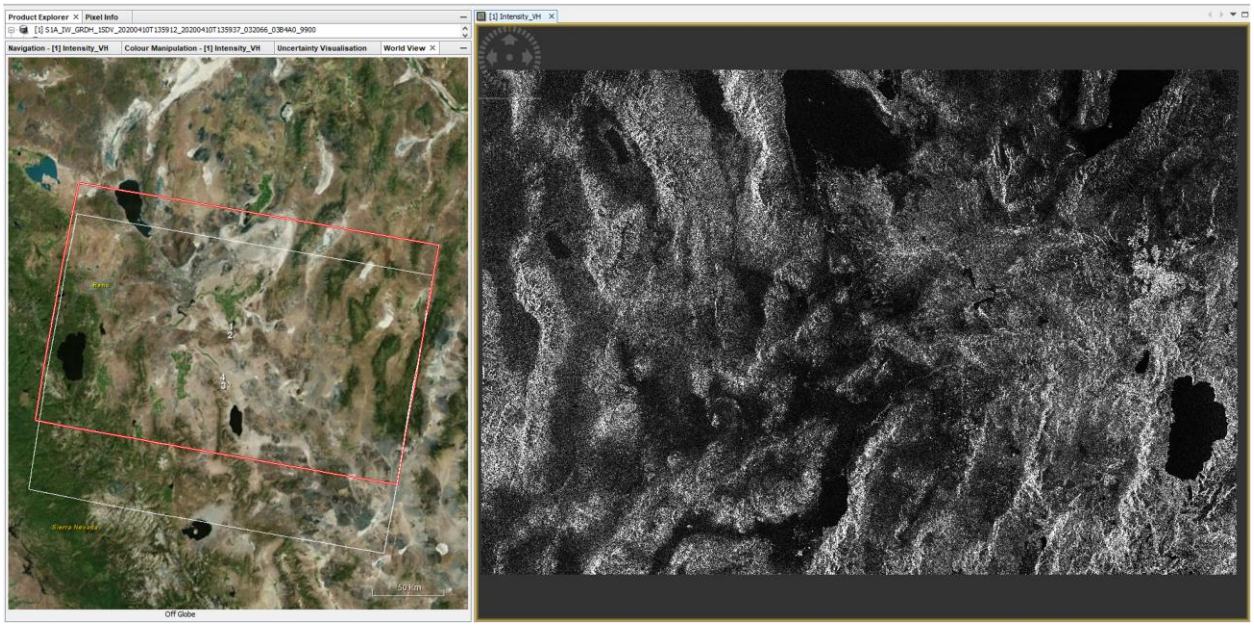

Figure 5. Visualization of the complex data using a virtual intensity band.

Step 3: Thermal noise removal (TNR) and apply orbit file

Sentinel Application Platform (SNAP) software provides a Thermal Noise Removal (TNR) module to remove thermal noise from the channel intensities of polarimetric Sentinel-1 data. To estimate the noise-free matrix, noise correction on the complex data is applied.

Apply precision orbit correction with Apply-Orbit-File (AOF). Orbit file data can be downloaded by S1TBX and include information about the accurate position of the satellite image during the acquisition of SAR data. The Precise Orbit Ephemerides (POE) orbit files cover approximately 28 hours and contain orbit state vectors at fixed time steps of 10-second intervals. The POE files are generated every day and delivered within 20 days after data acquisition.

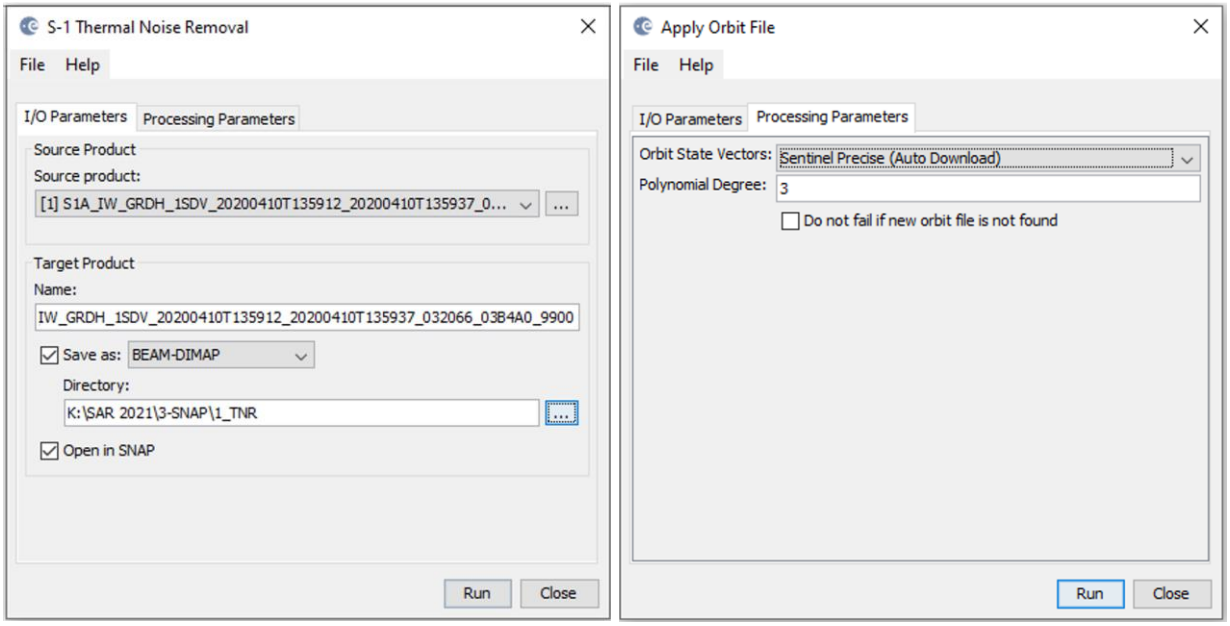

Figure 6. Thermal Noise Removal (TNR) module and apply orbit file

Step 4: Perform Border Noise Remove (BNR) and radiometric correction

The Sentinel-1 Ground Range Detected (GRD) product generated by the Instrument Processing Facility of the European Space Agency (ESA) has noise artifacts at the image borders of both left and right sides of the satellite's cross track. The Sentinel-1 border noise removal is important to mitigate backscatter from Sentinel-1 SAR data for time-series analysis and control SAR data quality for the large-scale data processing.

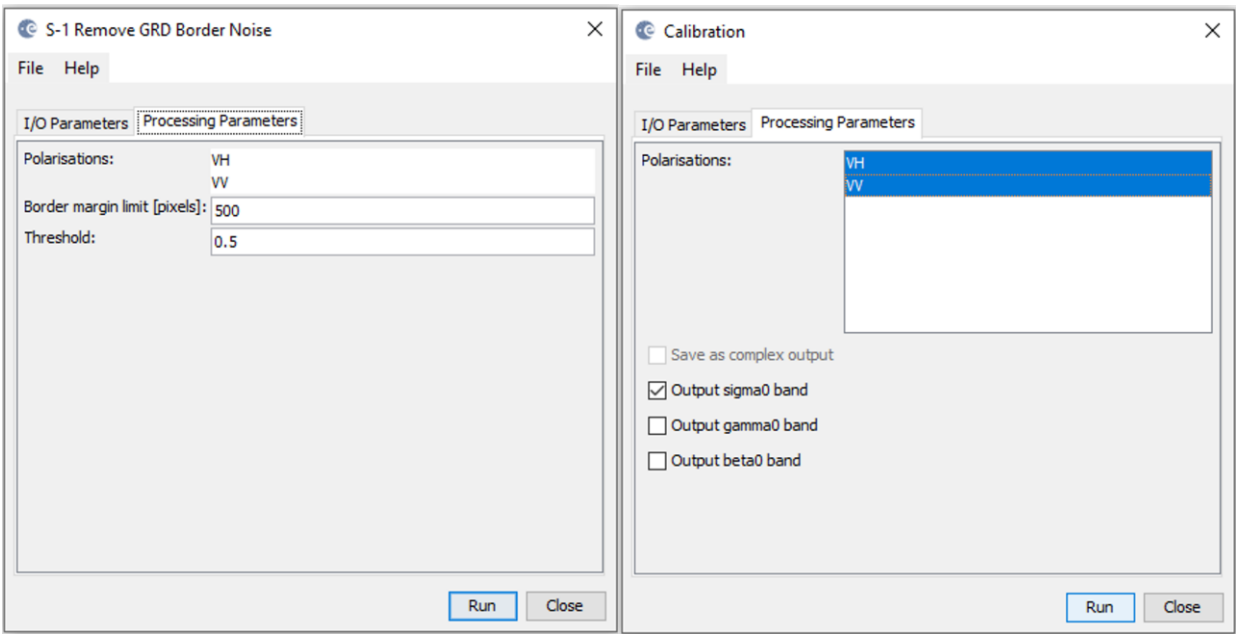

Figure 7. Border Noise Remove (BNR) and radiometric correction

Radiometric calibration or radiometric correction is to convert the raw digital image data recorded by satellite sensors into common physical scales based on known reflectance measurements taken on the ground's surface and avoid radiometric errors or distortions.

Step 5: Co-register the images

Image co-registration is conducted for the comparison of two or more images in a series to understand any change. For interferometric processing, multiple images must be co-registered into a stack. One image is selected as the reference or master and the other images are the slaves that all other images are aligned. The rationale of co-registration is to ensure that each ground target or image become aligned to the same range and azimuth pixel in both the master and the slave images.

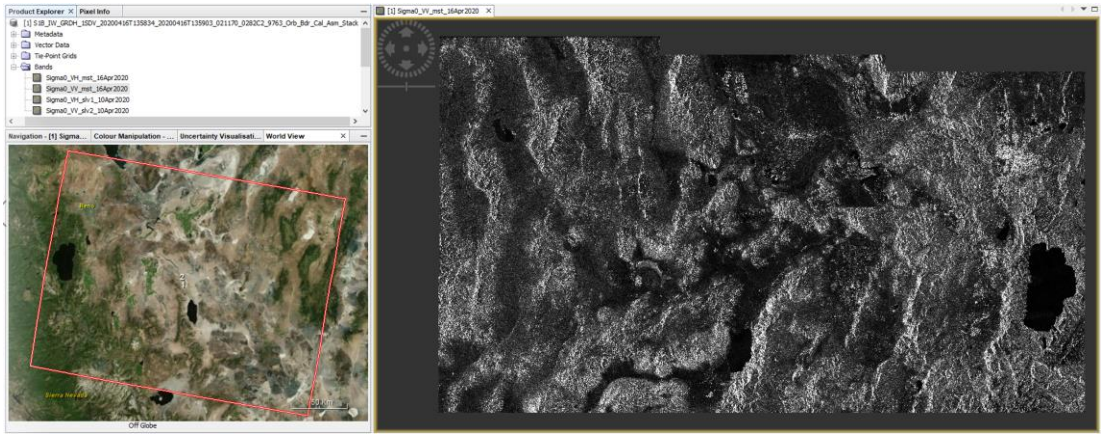

Figure 8. Co-registration of the images

Step 6: Multi-Temporal speckle filter

Radar image brightness is normally expressed in σ^o (sigma-nought) which is the radar backscatter per unit area. The unit of σ^o is [m^2/m^2], expressed in decibel (dB). Radar backscatter amplitude is provided as two separate images for the Horizontal- Horizontal (HH) and Horizontal-Vertical (HV) polarizations.

In order to accurately interpret the content of a SAR image, the radar polarization is a parameter to affect the strength of the backscatter. Current spaceborne radar systems operate with linear polarization where the radar signals are transmitted and received at horizontal (H) and/or vertical (V) polarization.

In general, speckle filtering allows a clear increase in the Equivalent Number of Looks (ENL) according to the filtering spatial resolution through a progressive smoothing of the speckle. Speckle filtering allows to improve slope estimation at the pixel scale. However, it implies a degradation of the multi-look pixel size.

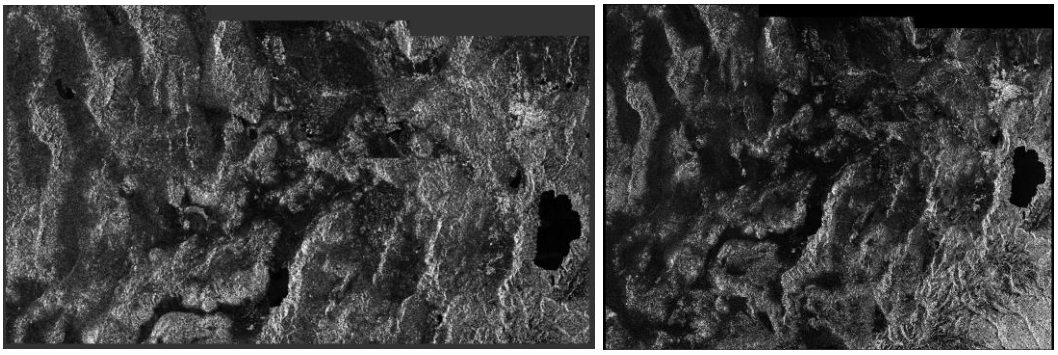

(a) (b)

Figure 9. Multi-Temporal speckle filter with the Lee filter: (a) raw Sentinel-1 L1C GRD VH band image delivered by ESA; (b) Same Sentinel-1 VH band after use of spatial Lee filter

Step 7: Terrain correction

Terrain correction removes the effect of variations in the observations due to the topography near observation sites and corrects geometric distortions that lead to geolocation errors. Topographic phase contributions are typically removed using a known Digital Elevation Model (DEM) to emphasize phases related to deformation. S1TBX will automatically find and download the DEM segment required for correcting your interferogram of interest.

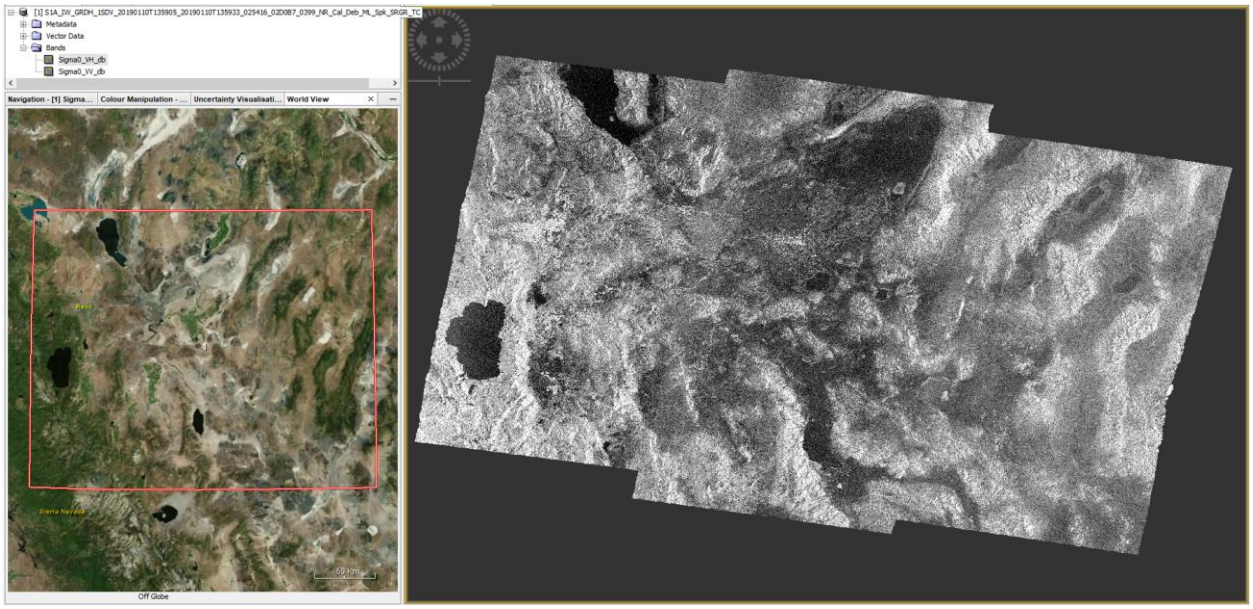

Figure 10. Range doppler terrain correction

Step 9: Export Data

The final geocoded data can be exported from S1TBX in a variety of formats with GeoTIFF, KMZ and various specialty formats.

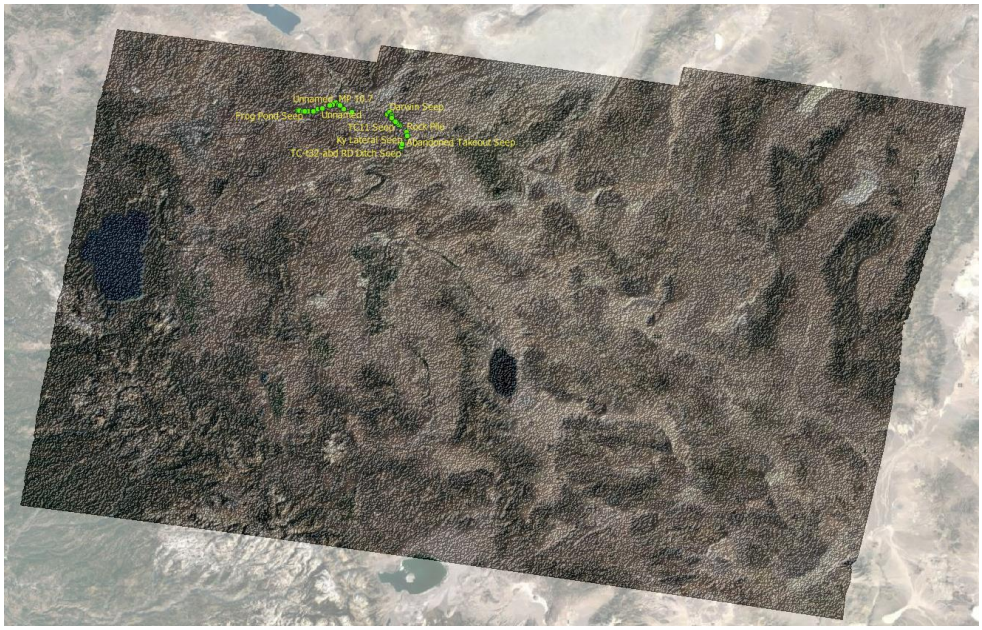

Figure 11. An image processed in the Truckee canal test site using SNAP

A full interferometry processing chain from dual-orbit Sentinel-1A and Sentinel-1B SAR data, open-source routines from the Sentinel Application Platform (SNAP), and Stanford Method for Persistent Scatterers (StaMPS) is introduced in Figure 24 (Mancini, et. al, 2021). The figure indicates that the processing of time series of displacements from a cluster of continuous global navigation satellite system stations can be used to provide a global reference frame for line-of-sight–projected velocities and validate velocity maps after the decomposition analysis.

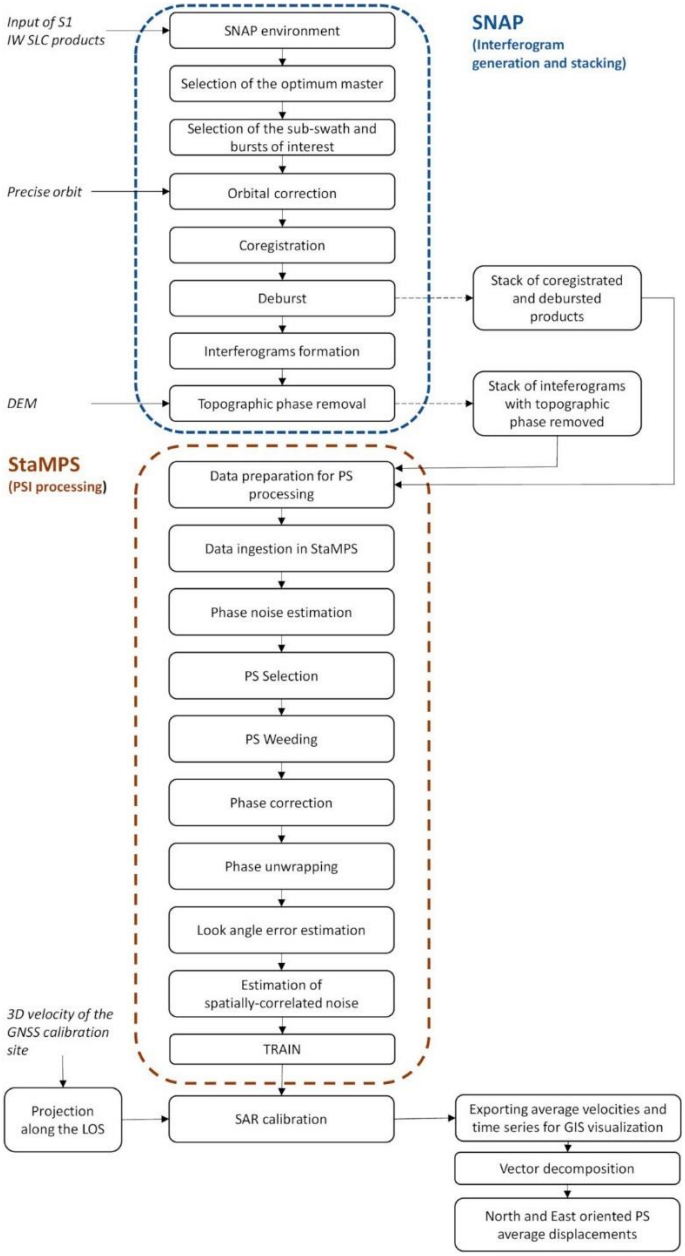

Figure 12. Combined SNAP–StaMPS workflow adopted in the present study for the S1 data processing (Mancini, et. al, 2021)

The processing of long-time series of displacements from continuous global navigation satellite system stations is used to provide a global reference frame for line-of-sight (LOS) velocities and validate

velocity maps after the decomposition analysis. Figure 25 shows that the combined Sentinel Application Platform (SNAP) and Stanford Method for Persistent Scatterers (StaMPS) workflow can be a reliable tool for S1 data processing based on the validation procedure (Mancini, et. al, 2021)

4.3 InSAR Scientific Computing Environment (ISCE)

The InSAR Scientific Computing Environment (ISCE) is a framework designed for the purpose of processing Interferometric Synthetic Aperture Radar (InSAR) data. The framework aspects of ISCE have been designed as a general software development framework. The ISCE is an open source with a modular software framework capable of supporting the geophysical research, InSAR data processing, and data modeling communities.

Applications of SAR are various and one of the principal applications of the SAR technology is represented by the interferometric SAR (InSAR) technique. The InSAR technique depends on the measurement of the phase difference between two or more complex SAR images acquired from different orbital positions and times.

The phase of the SAR image is a function of the distance between the satellite and the ground. It is determined primarily by the distance between the satellite antenna and the ground targets. The phase of each SAR image pixel carries range information to a small fraction of the SAR wavelength. The amplitude corresponds to the degree of strength of the radar backscatter and the phase corresponds to the position on a map where the data come from.

The SAR data processing consists of five major steps although not always in the following order: (1) SAR data collection, (2) data pre-processing, (3) interferogram generation, (4) phase unwrapping, and (5) geocoding.

Step 1. SAR data collection
Historical multiple-year L-band and C-band satellite image data archived from the ALOS-1(L-band) and Sentinel-1A/B (C-band) can be searched, accessed, and collected from the Seamless SAR Archive (SSARA) Federated Data Search and Access link.
(https://web-services.unavco.org/brokered/ssara/gui)

Step 2. Data pre-processing
Orbit data are used to compute offset vectors at pixel level from Single Look Complex (SLC) images. The effects of orbit positions and earth curvature are removed. Because the satellite is in different orbit positions for the two acquisitions, the distance between satellite and ground will vary across the image.

The processed image is resampled to the master grid. Two images from the same track and frame will be separated in time and still shifted slightly. Cross-correlate subsets of the two images using amplitude correlation to estimate the shift between the images.

Co-registered stacks of single-look complex (SLC) data can be created to generate surface displacement time-series followed by further analysis of the phase and amplitude. The process of

multi-looking is applied to reduce phase noises by the averaging of adjacent samples or low pass filtering of interferogram and to improve the SAR image quality by reducing the speckle.

Step 3. Interferogram generation

An interferogram is formed by multiplying one SLC image (master image) by the complex conjugate of the other SLC images (slave images). Interferometric products are computed to generate the complex interferogram and the coherence images. The interferometric phase can be corrected for the phase of a ground control reference point and coherence changes can be compared through time. Interferometric phase at each SAR image pixel, depends on the difference in the travel paths from the SAR sensor to the considered resolution cell during the acquisition of each image.

Step 4. Phase unwrapping

Unwrapping is the process of converting the cyclical phase signal from the interferogram into a smooth deformation signal. Several different algorithms exist for unwrapping. Original phase from the wrapped phase representation is reconstructed with a sophisticated phase unwrapping algorithm. The interferogram is filtered and unwrapped.

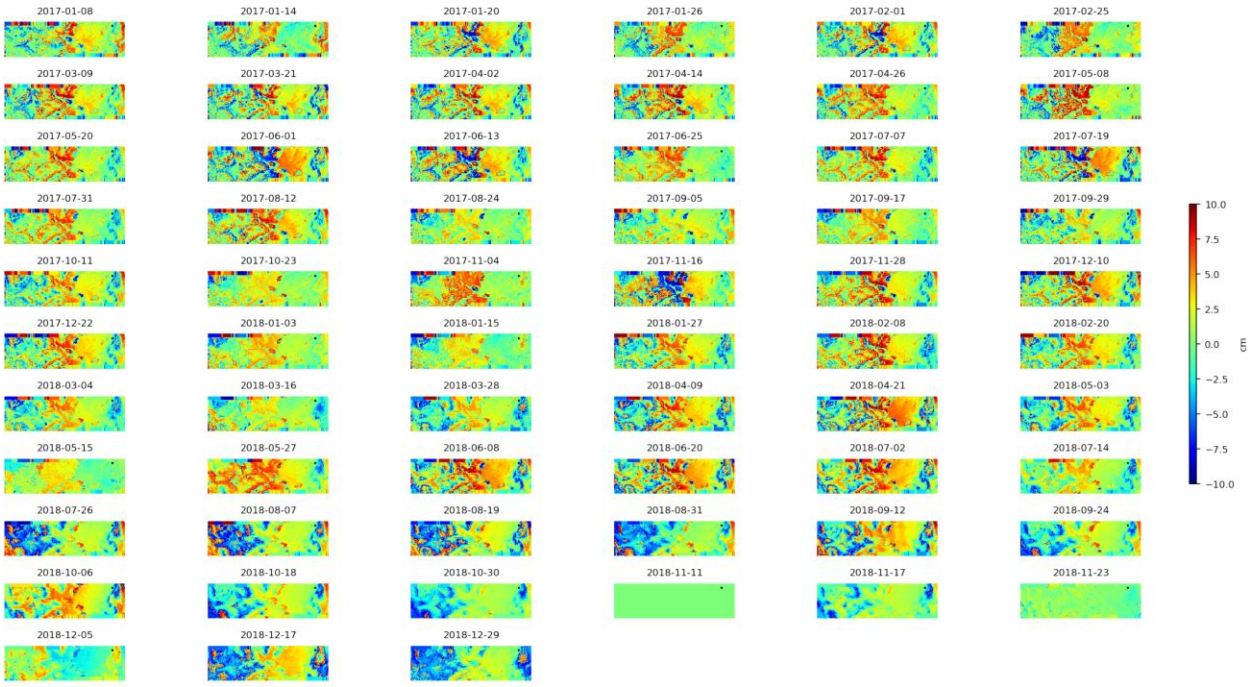

Figure 13. Wrapped phase timeseries at Truckee canal study site.

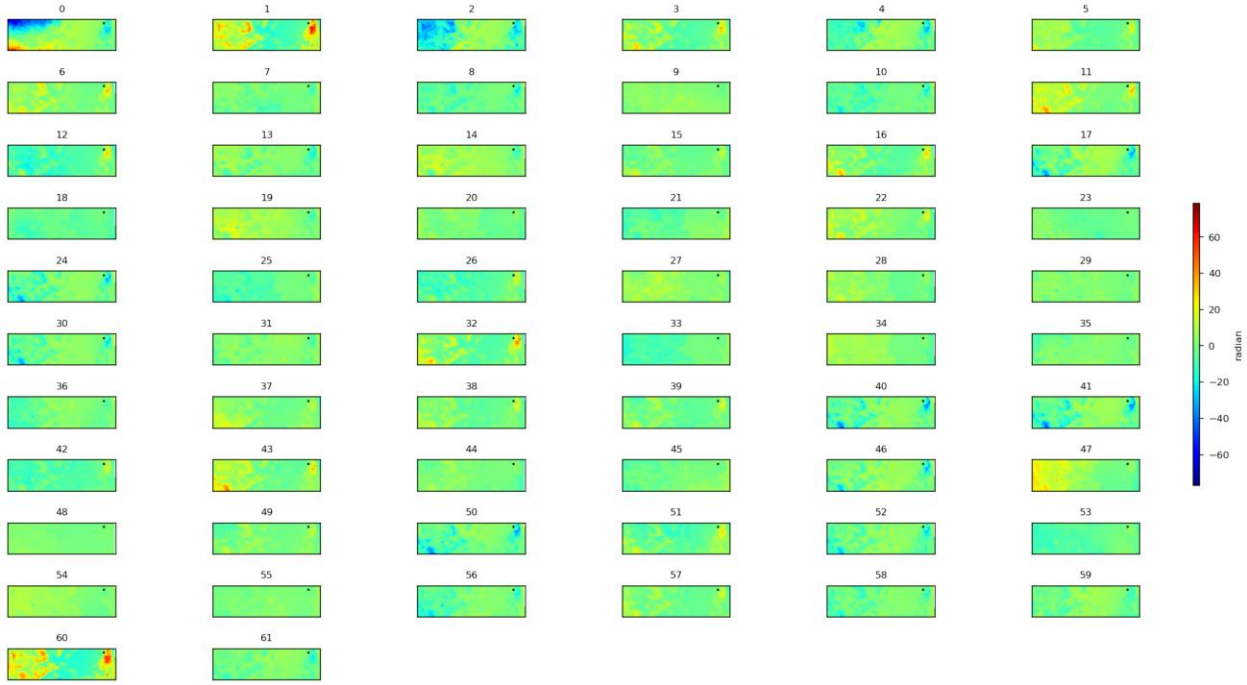

Figure 14. Unwrapped phase timeseries at Truckee canal study site.

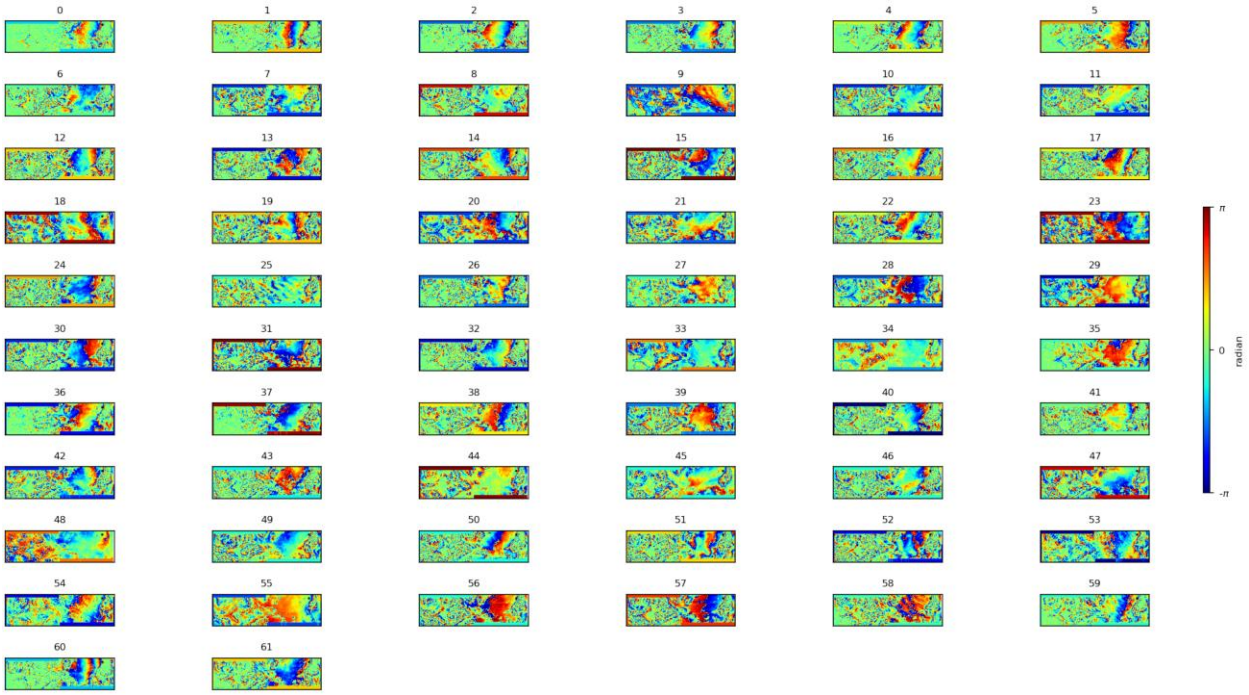

Figure 15. Unwrap phase and wrap checkpoint at Truckee canal study site.

Step 5. Geocoding

Unwrapped phase is converted to a height and the pixel coordinates are georeferenced. Interferogram is registered to a Digital Elevation Model (DEM) with forward or backward mapping to apply a topographic correction. The processing data are converted from radar coordinates of range and

azimuth to geographic coordinates for the final processing step. The generated products can be modified for contouring and layering with geographic information system (GIS) programs.

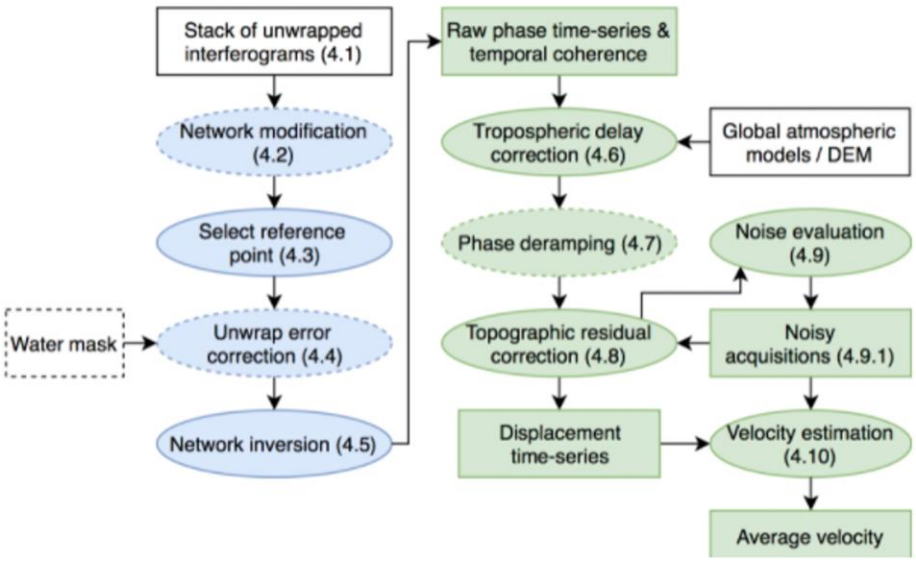

Figure 16. The routine processing workflow of InSAR time series analysis: (blue ovals) correcting unwrapping errors and inverting for the raw phase time-series and (green ovals) correcting for noise from different sources to obtain the displacement time-series (Yunjun et. al., 2019).

InSAR technique has solved various geodetic applications and ground deformation measurements. A new challenge is to monitor global surface deformation with high precision and large computing power. Figure 29 show the routine processing workflow of InSAR time series analysis. The MintPy script takes a stack of co-registered and unwrapped interferograms and generates the displacement time-series. The workflow consists of two main blocks: correcting unwrapping errors and inverting for the raw phase time-series (blue ovals) and correcting for noise from different sources to obtain the displacement time-series (green ovals).

For this research, the InSAR data processing was performed using the ISCE platform and MintPy time-series software was used for the InSAR time-series analysis in the project site.

MintPy is the Miami INsar Time-series software in Python. It is an open-source package for InSAR time series analysis. It reads the stack of interferograms (co-registered and unwrapped) in ISCE, ARIA, FRInGE, HyP3, GMTSAR, SNAP, GAMMA or ROI_PAC format, and produces three-dimensional (2D in space and 1D in time) ground surface displacement in line-of-sight (LOS) direction.

MintPy reads a stack of interferograms (unwrapped interferograms, coherence and connected components from SNAPHU if available) and the geometry files (DEM, lookup table, incidence angle, etc.). MintPy is modulized in Python with utilities classes and functions and well commented in the code level.

5. Results

5.1 VADOSE/W Hydraulic Model

Seepage analyses at some cross sections were conducted using the computer program VADOSE/W (GEO-SLOPE, 2012). VADOSE/W software is a finite element program that can be used to model movement and distribution of pore water within porous materials such as soil and bedrock. VADOSE/W can model both saturated and unsaturated flow in response to climatic conditions making it possible to analyze seepage as a function of time while considering infiltration, precipitation, surface water runoff and ponding, plant transpiration, actual evaporation, and heat flow.

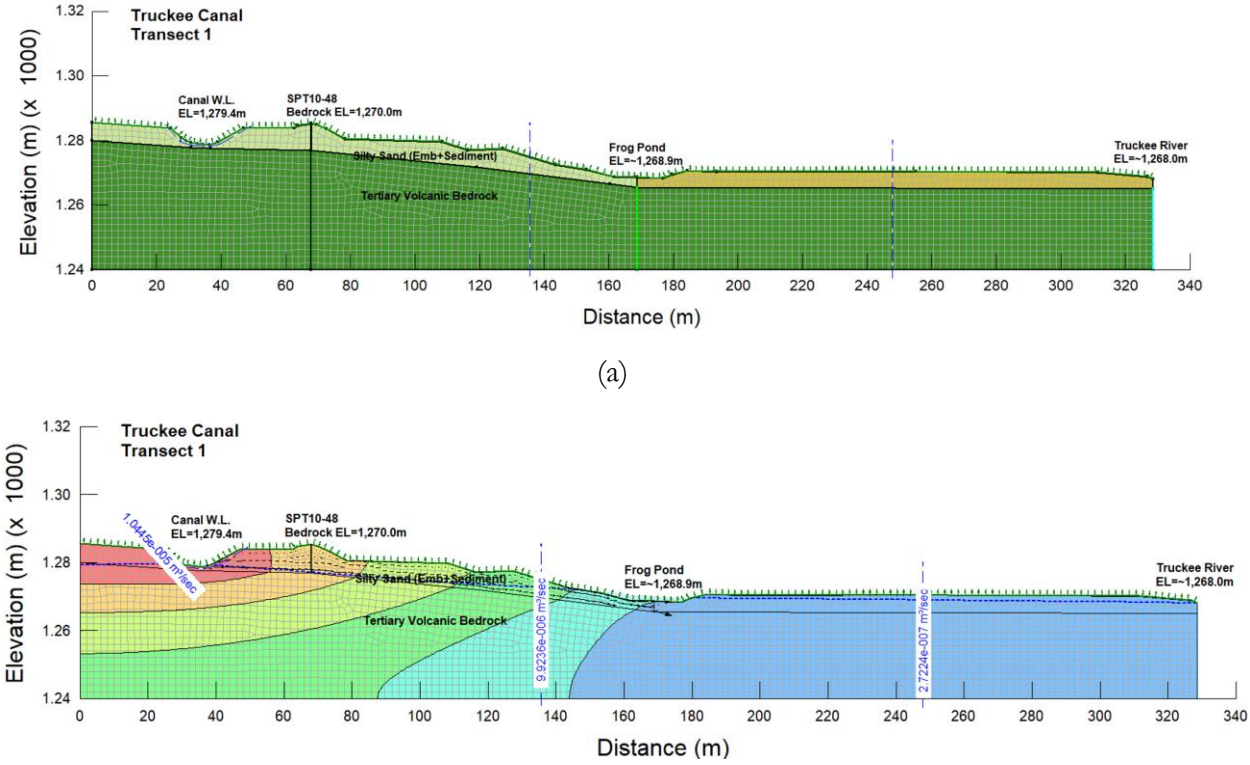

Figure 17. Modeling domain geometry (a) and total head contour (b) at transect 1 using VADOSW/W

As an example of VADOSE/W hydraulic models, Figure 17 shows the geometry of a cross section view (a) and total head contours (b) simulated using the VADOSE/W modeling program.

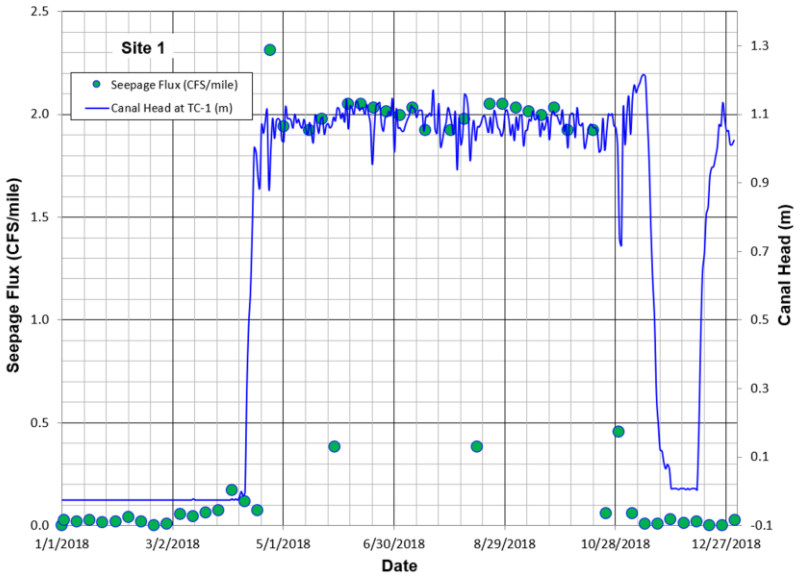

Figure 18. Comparison of canal head vs seepage flux.

Figure 18 shows the comparison of canal head and seepage flux values estimated from the VADOSE/W modeling at site 1. The results at site 1 location indicates that corresponding dates of canal watering-up/de-watering correlate with the changes of seepage flux values.

The results of the seepage loss rates estimated VADOSE/W models are summarized in Table 1.

Table 1. Summary of VADOSW/W modeling results

	Time	Total Flow In Total	Per linear meter	Conversion (hr to sec)	Conversion (ft^2 to m^2)		VADOSE/W Models
	T(hr)	Total Flux(m^2/hr)	Cumulative Flux(m^3/hr)	1hr/(60*60)sec	(3.28feet/1m)^2	Cumulative Q(ft^3/s)	Cumulative Q(CFS per mile)
Site1	5374	6.3E+02	**1.2E-01**	2.8E-04	10.76	3.5E-04	**2.0**
Site2	5525	2.1E+01	**3.8E-03**	2.8E-04	10.76	1.1E-05	**0.2**
Site3	5428	5.4E+02	**1.0E-01**	2.8E-04	10.76	3.0E-04	**1.5**
Site4	2500	9.2E+02	**3.7E-01**	2.8E-04	10.76	1.1E-03	**2.8**
Site5	2500	5.1E+02	**2.0E-01**	2.8E-04	10.76	6.1E-04	**2.6**
Site6	2500	3.2E+02	**1.3E-01**	2.8E-04	10.76	3.9E-04	**1.3**
Site7	2500	2.2E+02	**8.9E-02**	2.8E-04	10.76	2.7E-04	**1.2**
Site8	2500	1.5E+02	**6.0E-02**	2.8E-04	10.76	1.8E-04	**1.5**
Site9	2500	2.1E+02	**8.2E-02**	2.8E-04	10.76	2.5E-04	**0.7**
Site10	2500	1.1E+02	**4.3E-02**	2.8E-04	10.76	1.3E-04	**0.2**
Site11	2500	4.6E+01	**1.8E-02**	2.8E-04	10.76	5.5E-05	**0.1**
Site12	2500	9.4E+01	**3.7E-02**	2.8E-04	10.76	1.1E-04	**0.2**
Site13	2500	1.1E+02	**4.4E-02**	2.8E-04	10.76	1.3E-04	**0.2**
Site14	2500	4.2E+02	**1.7E-01**	2.8E-04	10.76	5.0E-04	**2.1**
Site15	2500	1.2E+02	**4.8E-02**	2.8E-04	10.76	1.4E-04	**0.2**

Slug tests were performed at Truckee canal monitoring wells and piezometers. A slug test estimates the hydraulic properties of aquifer formations. A slug test raises or lowers the groundwater level in a

well bore by injecting or removing a known slug volume. The water level response during rising head or falling head displacements is recorded with elapsed time using a transducer.

The advantages of a slug test are that (1) it is quick and easy to perform (e.g., a test can be completed within a few minutes), (2) has a low cost (e.g., many tests can be performed in a single day), (3) only the test well is needed (no other observation wells), and (4) no pumping is required, and therefore, no water is produced (which is good for hydrogeologic investigations of contaminated sites). The disadvantages of a slug test are (1) it only evaluates a small portion of the aquifer (pumping tests provide a more regional estimate of aquifer conductivity) and (2) results may be profoundly affected by the gravel pack in the borehole adjacent to the well screen.

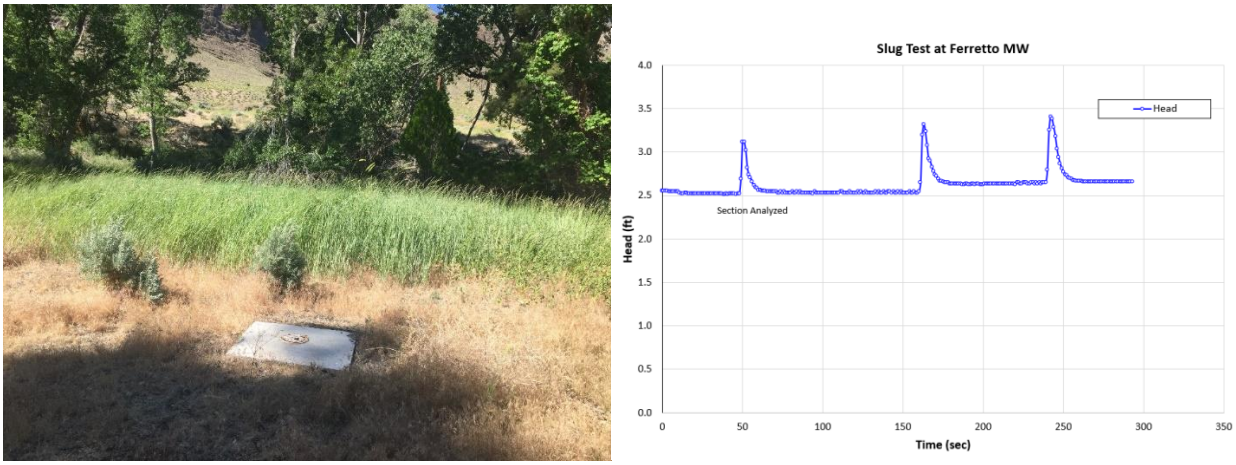

Figure 19. Slug test conducted at a Ferretto monitoring well in the Truckee Canal: (a) photo of monitoring well; (b) raw data obtained the slug testing program.

As an example, the plots of the time-drawdown analysis results calculated for the Bouwer-Rice and Springer Gelhar methods conducted at a Ferretto monitoring well in the Truckee canal are shown in Figures 20.

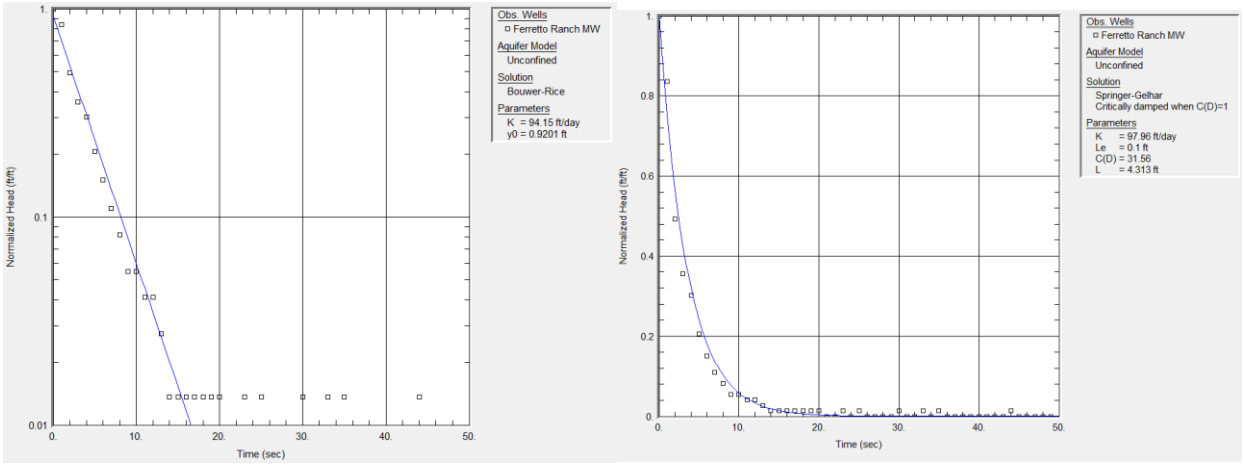

Figure 20. Normalized water-level displacement as a function of time with (a) Bouwer and Rice and (b) Springer Gelhar best-fit type curves at a Ferretto monitoring well in the Truckee Canal

Analysis of the slug tests was performed by the following methods: (1) Bouwer-Rice (1976), (2) Springer-Gelhar (1991), and KGS Model (1994) (HydroSOLVE, 2007). The information of identified monitoring wells and piezometers is summarized in Table 2. The results of the hydrogeological parameters estimated using the AQTESOLV program at the monitoring wells and piezometers are summarized in Table 3.

Table 2. Truckee canal monitoring wells and piezometers

Name	Type	Nearest USGS Site ID	CasingDiameter_IN	TotalDepth_FT	PerfStart_FT	PerfEnd_FT	WL-BLSD_FT	WL_Date
SPT-10-50, OW-1	Monitoring Well	Site 2	1.5	23.5	13.5	23.5	19.74	5/30/2019
NA	Monitoring Well	Site 6	2	23.5	13.5	23.5	18.31	5/30/2019
SPT-10-38, OW-8	Monitoring Well	Red Barn Seep	1.5	16.0	5	15	10.37	5/21/2019
Site12_Domestic	Domestic Well	Site 12 Domestic	6 5/8	Unknown	Unknown	Unknown	27.27	4/23/2019
SPT-10-36, OW-7	Monitoring Well	Site 10	1.5	28.5	15	25	22.96	5/21/2019
Feretto Rach MW	Monitoring Well	Site 1, Frog Pond Seep	2	Unknown	Unknown	Unknown	5.94	5/21/2019
Frog Pond Piezo	Piezometer	Site 1	1	8.1	7.6	7.9	-0.1	5/21/2019
Site 13 Piezo	Piezometer	Site 13	1	3.7	3.2	3.5	2.74	5/30/2019
Site 12 Piezo	Piezometer	Site 12 Domestic	1	5.4	4.9	5.3	3.31	5/30/2019
Site 11 Piezo	Piezometer	Site 11	1	4.0	3.5	3.8	3.91	5/30/2019
Site 9.5 Piezo	Piezometer	Site 9.5	1	6.3	5.8	6.1	4.05	5/30/2019
Site 9 Piezo	Piezometer	Site 9	1	3.4	2.9	3.2	3.27	5/30/2019
Site 6 Piezo	Piezometer	Site 6	1	3.9	3.4	3.8	2.12	5/30/2019
Site 5 Piezo	Piezometer	Site 5	1	4.4	3.9	4.3	3.36	5/30/2019

Table 3. Summary of slug test analyses results

Well ID	Analysis Method	Hydraulic Conductivity	Avg. Hydraulic Conductivity
Ferretto Ranch MW	Bouwer-Rice (1976)	94.2	103.7
	Springer-Gelhar (1991)	98.0	
	KGS Model (1994)	119.1	
Site 1 (Frog Pond)	Bouwer-Rice (1976)	1.1	1.2
	Springer-Gelhar (1991)	1.2	
	KGS Model (1994)	1.2	
Site 2 (OW-1, SPT-10-50)	Bouwer-Rice (1976)	28.5	42.9
	Springer-Gelhar (1991)	43.8	
	KGS Model (1994)	56.4	
Site 6 (N/A)	Bouwer-Rice (1976)	2.4	2.7
	Springer-Gelhar (1991)	3.4	
	KGS Model (1994)	2.5	
Site 9.5	Bouwer-Rice (1976)	2.30	2.2
	Springer-Gelhar (1991)	2.09	
	KGS Model (1994)	2.27	
Site 11	Bouwer-Rice (1976)	0.33	0.4
	Springer-Gelhar (1991)	0.42	
	KGS Model (1994)	0.48	
OW-8 (SPT-10-38, Red Barn Seep)	Bouwer-Rice (1976)	0.96	1.5
	Springer-Gelhar (1991)	1.66	
	KGS Model (1994)	1.85	
Site 12	Bouwer-Rice (1976)	1.5	2.2
	Springer-Gelhar (1991)	2.6	
	KGS Model (1994)	2.5	

Average values of the hydraulic conductivity (K) estimated from slug tests conducted at the monitoring wells and piezometers range from 0.4 to103.7 ft/day. The slug test results indicate that the aquifer system at a Ferretto monitoring is pervious with sand and gravel materials. The hydraulic

conductivity (K) estimated from the other monitoring wells and piezometers indicate semi-pervious geologic formation.

5.2 InSAR Data Processing Results

For this research, C-band Sentinel-1A and -1B satellite imagery data with historical 6- or 12-day repeat cycles are collected to cover a project site and analyzed for the timeseries analysis. Even though L-band Advanced Land Observing Satellite (ALOS) imagery data was collected, the data was not used for timeseries analysis because historical satellite imagery acquisitions are planned with 46-day repeat cycles since the timing of acquisitions easily miss to capture any seep events.

The nature of radar scattering is a function of the wavelengths of the features on the surface. A radar wavelength shorter than the features results in a brighter image. Backscatter is the term used to describe the variety of reflection angles resulting from the radar bounce. The backscatter is a function of the incidence angle, θ. The radar return is a function of slope, roughness and dielectric constant.

A satellite emits a radar pulse. The radar is backscattered. Amplitude and phase of echo (return) are recorded at the satellite. At angles less than 30 degrees, backscatter is dominated by slope; it is dominated by roughness between 30 and 70 degrees; after that shadowing becomes a problem. Slopes nearly orthogonal to the radar pulse reflect more brightly than those at a steeper angle. Terrain roughness is defined by the RMS of height variation relative to the radar wavelength.

Brighter areas on the image means rougher terrain. Moisture increases dielectric constant, increasing reflectivity and pixel brightness. This varies with material as well. SAR images also inherently contain noise, often called speckle. Speckle manifests as the apparently random placement of conspicuously bright or dark pixels.

Line of sight (LOS) is the level of obstruction on the path between two points. The level of obstruction in a LOS determines not only the visibility from one point to another but also the quality of signal reception for wireless transmissions.

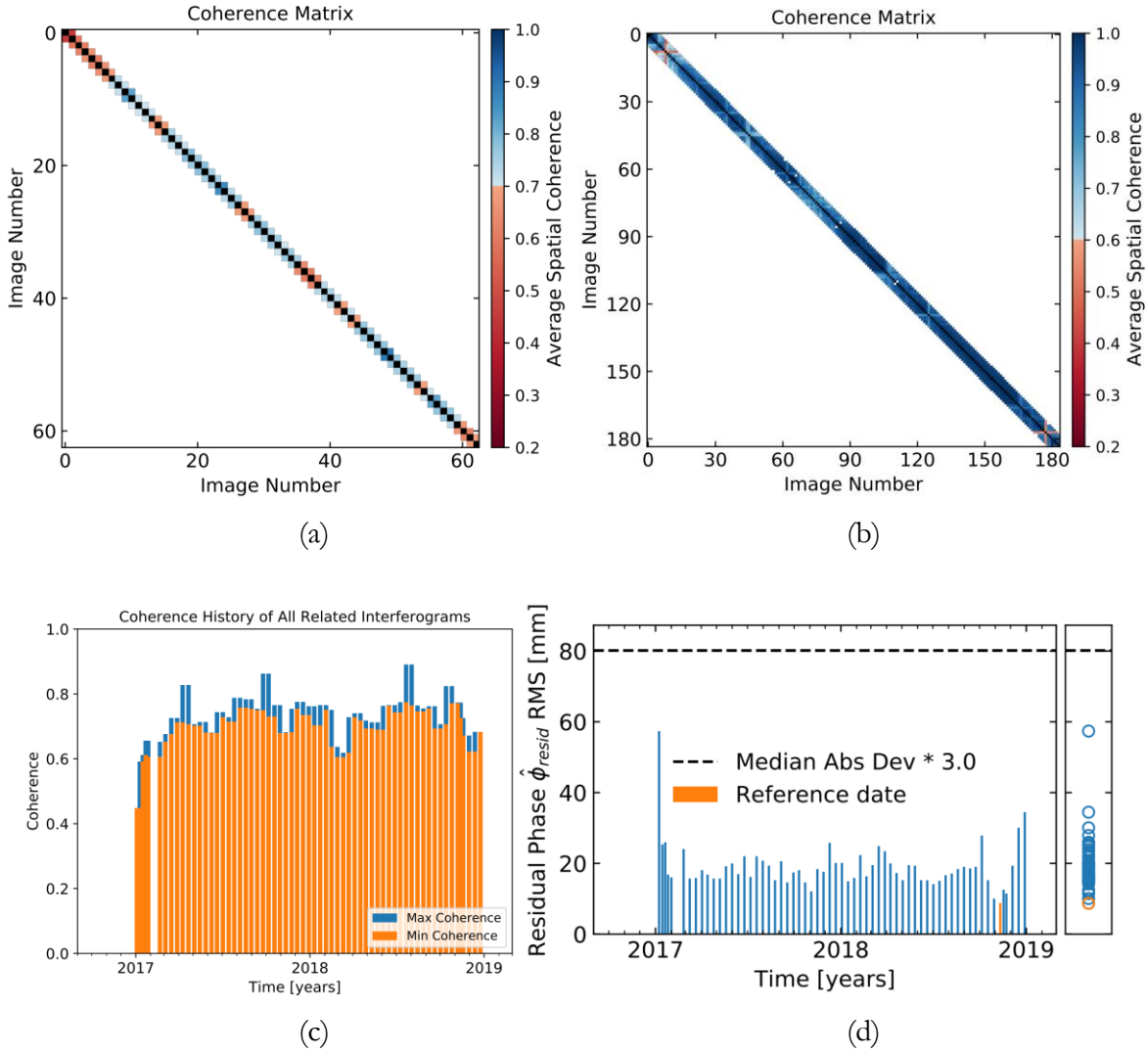

Figure 21. Simulations for weight functions performance assessment in InSAR data processing: (a) Simulated unwrapped phase; (b) Spatial coherence; (c) Coherence as a function of time; and (d) Root Mean Square (RMS) of residual phase timeseries as a function of time.

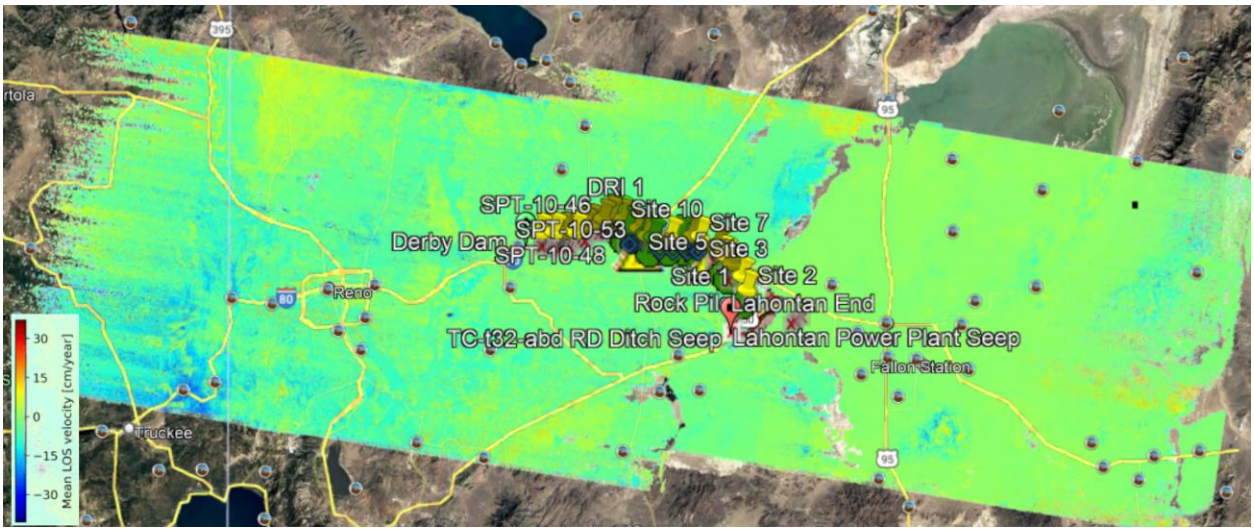

Figure 22. Mean line-of-sight (LOS) velocity (cm/year) map obtained from InSAR data processing at Truckee canal study domain for 2017 and 2018.

The Sentinel-1 SAR imagery data with acquisition cycles of 6 to12 days were used for this research, the InSAR data processing results at known seep locations indicates that corresponding dates of canal watering-up/de-watering correlate with the changes of SAR mean line-of-sight (LOS) velocity (mm/year) values obtain from timeseries analysis at known seep locations. However, still the Sentinel-1 SAR imagery data have relatively low spatial resolution for detecting the small scale of the seeps.

Volumetric water contents were measured at the seep locations using a portable handheld probe (HS2P HydroSense II) during irrigation season. In 2019, the soil moisture content remained dry due to low stage and flow in the canal. In 2020, the soil water content increased along with canal flow.

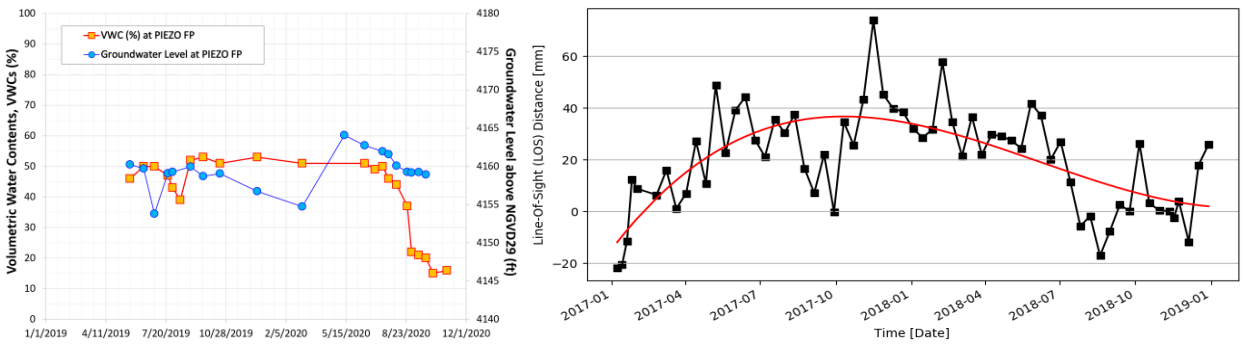

(a) (b)

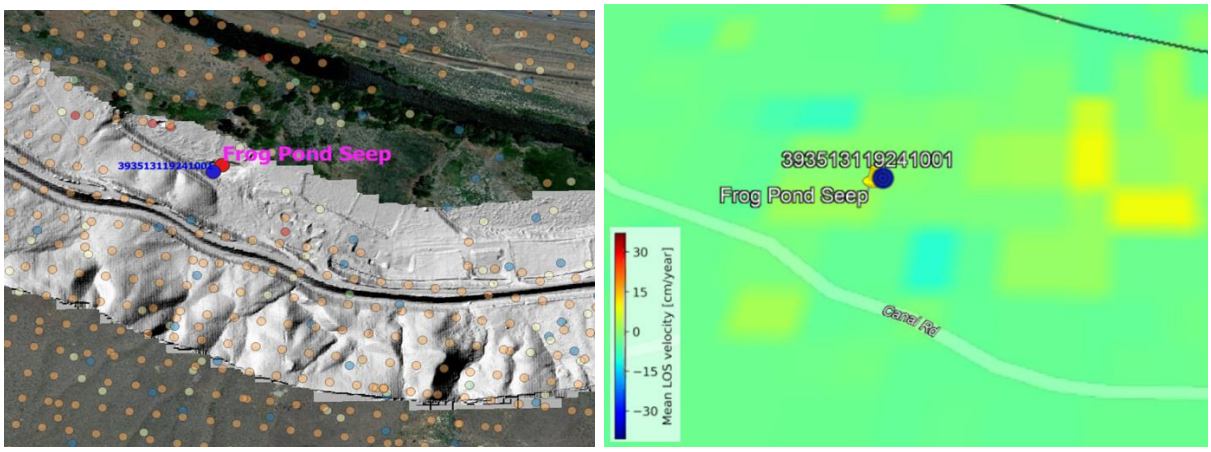

(c) (d)

Figure 23. InSAR data processing at Frog Pond Seep (Piezo FP, USGS 393513119241001): (a) Soil water content measured at the seep location (b) Time series of mean line-of-sight (LOS) distance (mm); (c) Identified known seepage sites; and (c) Mean line-of-sight (LOS) velocity (cm/year).

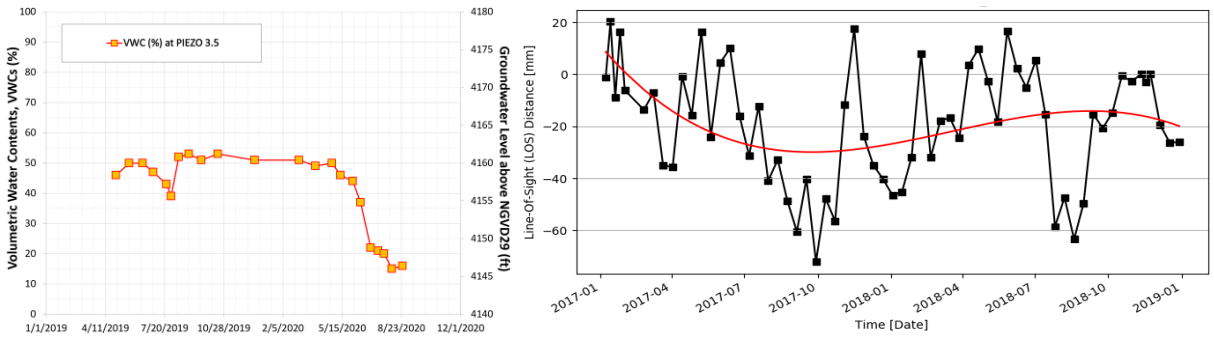

(a) (b)

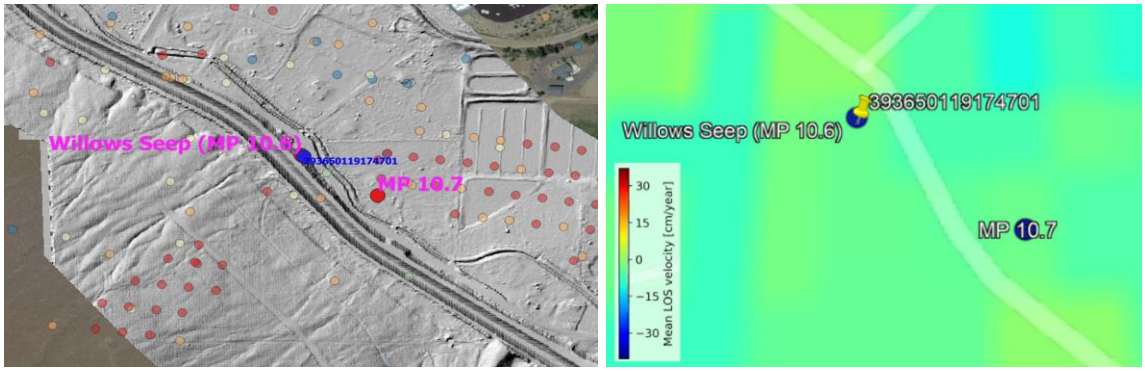

(c) (d)

Figure 24. InSAR data processing at Willows Seep (Piezo 3.5, USGS 393650119174701): (a) Soil

water content measured at the seep location (b) Time series of mean line-of-sight (LOS) distance (mm); (c) Identified known seepage sites; and (c) Mean line-of-sight (LOS) velocity (cm/year).

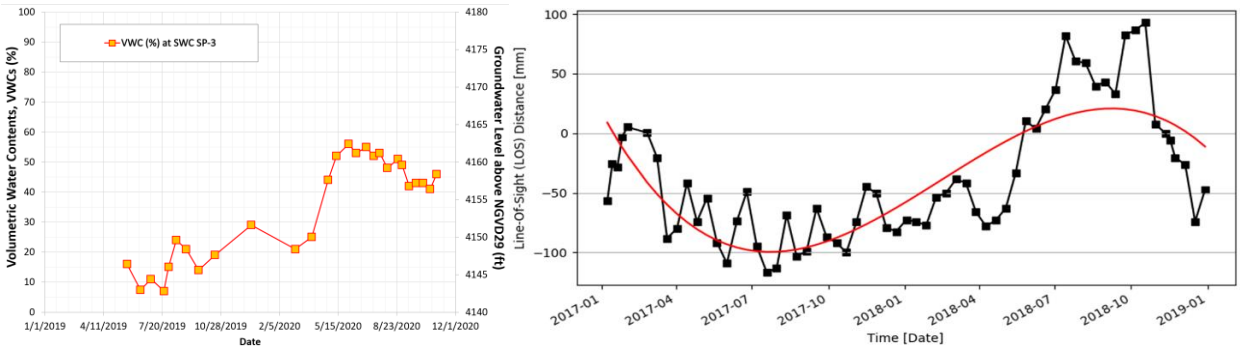

(a) (b)

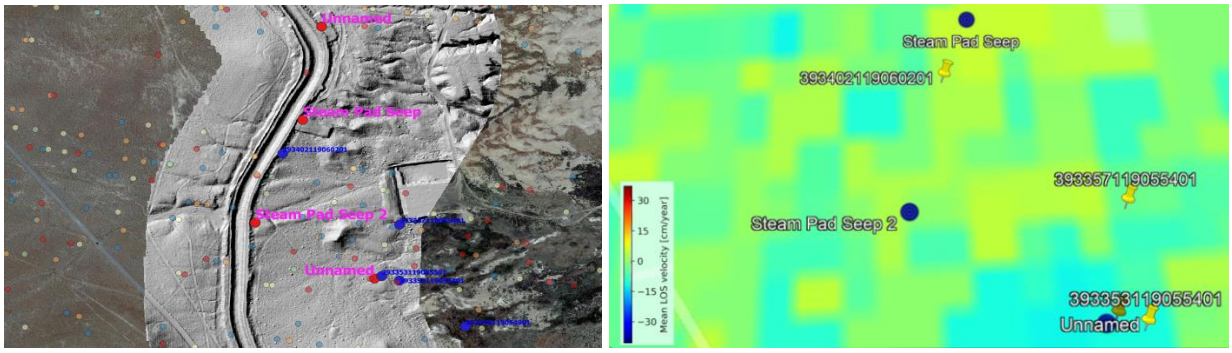

(c) (d)

Figure 25. InSAR data processing at Steam Pad Seep (SWC SP-4, USGS 393438119065401): (a) Soil water content measured at the seep location (b) Time series of mean line-of-sight (LOS) distance (mm); (c) Identified known seepage sites; and (c) Mean line-of-sight (LOS) velocity (cm/year).

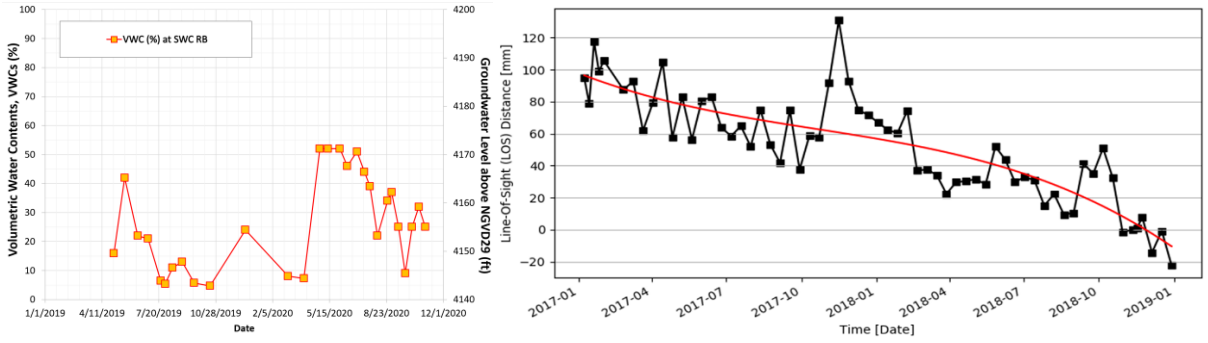

(a) (b)

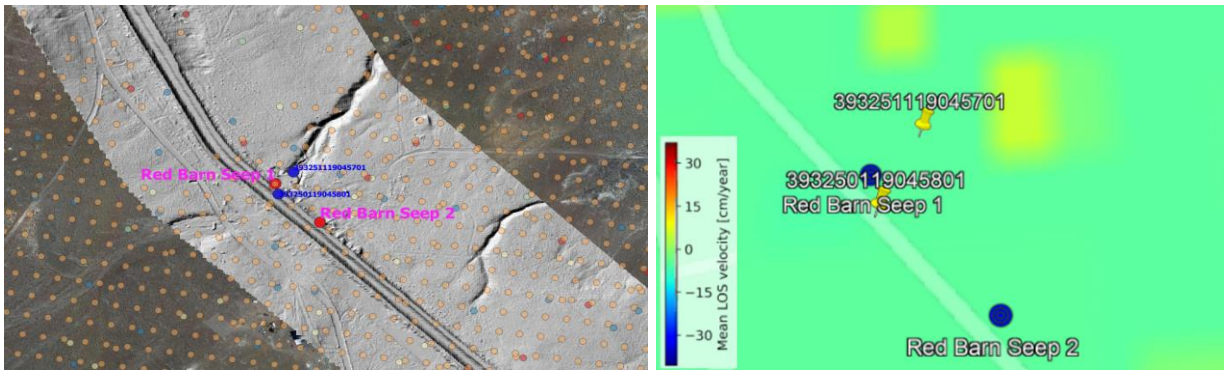

(c) (d)

Figure 26. InSAR data processing at Red Barn Seep1 (SWC RB, USGS 393251119045701): (a) Soil water content measured at the seep location (b) Time series of mean line-of-sight (LOS) distance (mm); (c) Identified known seepage sites; and (c) Mean line-of-sight (LOS) velocity (cm/year).

The InSAR data processing results at Frog pond, Willows, Stream Pad, and Red Barn known seep locations are presented in Figures 23 through 26. The results indicate that volumetric water contents were measured during irrigation season at the seep locations is corresponded with the mean line-of-sight (LOS) values and the soil water content patten is matched along with groundwater levels measured in Frog pond.

6. Discussions

Satellite frequency bands with high resolutions to detect seepage:

Airborne and spaceborne radar systems operate at various radar bands:

- P-band: ~69.0 cm (BIOMASS)
- L-band: ~23.5 cm (ALOS -2 PALSAR-2, SAOCOM-1, NISAR-L)
- S-band: ~9.4 cm (NovaSAR, NISAR-S)
- C-band: ~5.6 cm (Sentinel-1, Radarsat-2, RCM)
- X-band: ~3.1 cm (TerraSAR-X, TanDEM-X, COSMO-SkyMed)

Objects significantly smaller than the radar wavelength, become transparent to the radar, although they cause certain reduction of the amplitude of the signal. The smaller the objects, the less influence on the backscatter. L-band radar with longer wavelength radar signals consequently penetrate through the forest canopy since the small leaves are transparent and interact with the larger structures such as the larger branches of trees. On the other hand, C-band radar operating system at shorter wavelengths than L-band are more sensitive to sparse and low biomass vegetation.

For future research to conduct InSAR data processing, it is recommended use high spatial resolution data acquired from P-band for seepage detection; although, the use of P-band is limited to airborne deployments or apply L-band radar that penetrates the vegetation and soil to detect the seeps under the vegetation coverage. Proxy measurements like coherence change detection and NDVI are

possible future approaches for combining remote sensing techniques to detect seeps rather than directly measuring soil moisture.

SAR and InSAR combination for detecting soil moisture:

SAR alone may not be processed with any accuracy for soil moisture. The SMAP-Sentinel hybrid product is 3km and 0-5 cm depth. SAR by itself is very speckled and hard to resolve even wet from dry. The specking is from backscattering of vegetation and surface roughness. Change detection has been applied with limited success – but using passive microwaves to 'tie-down' the aggregate VWC at 9km, the SAR to scale the heterogeneity. However, the georeferencing in Sentinel has been found too poor for this as of late – at 1km. It would not work at approximately 10 m at this time for soil moisture and vegetation that's growing and changing would have an effect on the backscatter. If this technology is not ready, the upcoming NISAR mission will likely improve the georectification issues. They are working on a soil moisture retrieval algorithm, but it will be at 0-5cm depth and most likely at 100 or 200 m, not native resolution which is 10 m. It is particularly poor in agricultural lands where crop growth affects surface roughness. Vegetation growth around canal (and irrigated lands) would have similar impacts on retrievals around canals.

Characteristics of radar remote sensing have advantages compared to optical remote sensing as follows: (1) all weather capability (small sensitivity of clouds, light rain), (2) day and night operation (independence of sun illumination), (3) no effects of atmospheric constituents (multitemporal analysis), (4) sensitivity to dielectric properties (water content, biomass, ice), (5) sensitivity to surface roughness (ocean wind speed), (6) accurate measurements of distance (interferometry), (7) sensitivity to man-made objects, (8) sensitivity to target structure (use of polarimetry), and (9) subsurface penetration. The radar remote sensing also has inconvenient factors as follows: (1) complex interactions (difficulty in understanding, complex processing), (2) speckle effects (difficulty in visual interpretation), (3) topographic effects, and (4) effects of surface roughness.

7. Conclusions and Recommendations

InSAR remote sensing technology holds the potential to help identify unknown seepage, validate suspected canal seepage to differentiate from natural groundwater flow not related to canal losses, and identify changes in hydrologic parameters of interest such as hydraulic conductivity of canal embankments and foundation materials that may indicate progression of seepage pathways and internal erosion. This research serves the interests of any Reclamation region or office that has water conveyance or storage infrastructure and will benefit from the use of InSAR data processing platform technologies performed by this research.

The ALOS-1 SAR imagery data has very sparse acquisitions of about 3 to 4 per year and not sufficient for soil moisture or correlation time series analysis since the timing of acquisitions easily miss to capture any seep events. So, the Sentinel-1 SAR imagery data with more frequent acquisitions of 6 to12 days were used for this research, the InSAR data processing results at known seep locations indicates that corresponding dates of canal watering-up/de-watering correlate with the changes of SAR mean line-of-sight (LOS) velocity (mm/year) values obtain from timeseries analysis at known seep locations. However, still the Sentinel-1 SAR imagery data have relatively low

spatial resolution for detecting the small scale of the seeps. Indirect measurements such as coherence change detection and NDVI are potential future approaches for combining remote sensing techniques to detect any potential seeps.

For future research, the radar observation technique using high spatial resolution of airborne Uninhabited Aerial Vehicle Synthetic Aperture Radar (UAVSAR) can be feasible for filling in the gap between Reclamation's water conservation mission and a seepage monitoring algorithm tool. Image fusion between airborne and spaceborne scenes is another way to improve the spatial resolution of the spaceborne SAR images. The enhanced SAR monitoring algorithm tool can be developed and the expertise in soil moisture retrieval and disturbance detection will efficiently identify the leaks from the canal infrastructures managed by Reclamation.

References

Agapiou, A., D. D. Alexakis, K. Themistocleous, and D. G. Hadjimitsis (2016), Water leakage detection using remote sensing, field spectroscopy and GIS in semiarid areas of Cyprus, Urban Water Journal, 13(3), 221-231, doi:10.1080/1573062x.2014.975726.

Arshad, M., R. Gomez, A. Falconer, W. Roper, and M. Summers (2014), A remote sensing technique detecting and identifying water activity sites along irrigation canals, American Journal of Environmental Engineering and Science, 1, 19-35.

Bauer-Marschallingere, B., et al. (2019), Toward Global Soil Moisture Monitoring With Sentinel-1: Harnessing Assets and Overcoming Obstacles, Ieee Transactions on Geoscience and Remote Sensing, 57(1), 520-539, doi:10.1109/tgrs.2018.2858004.

Biggs J. and Wright T.J. (2020), How satellite InSAR has grown from opportunistic science to routine monitoring over the last decade, Nature Communications, https://doi.org/10.1038/s41467-020-17587-6.

Das, N. N. et al. (2011). "An Algorithm for Merging SMAP Radiometer and Radar Data for High-Resolution Soil-Moisture Retrieval." IEEE Transactions on Geoscience and Remote Sensing 49: 1504-1512.

Das, Narendra N. et al. (2014). "Tests of the SMAP Combined Radar and Radiometer Algorithm Using Airborne Field Campaign Observations and Simulated Data." IEEE Transactions on Geoscience and Remote Sensing 52: 2018-2028.

Di Martino, G., A. Di Simone, A. Iodice, and D. Riccio (2016), Scattering-Based Nonlocal Means SAR Despeckling, Ieee Transactions on Geoscience and Remote Sensing, 54(6), 3574-3588, doi:10.1109/tgrs.2016.2520309.

Duan, W.; Zhan, H.; Wang, C.; Tang, Y., (2021), Multi-Temporal InSAR Parallel Processing for Sentinel-1 Large-Scale Surface Deformation Mapping. Remote Sens. 2020, 12, 3749.

Fattahi, H., P. Agram, and M. Simons (2016), A Network-Based Enhanced Spectral Diversity Approach for TOPS Time-Series Analysis, IEEE Transactions on Geoscience and Remote Sensing, 55(2), 777-786, doi:10.1109/TGRS.2016.2614925.

GEO-SLOPE International, Ltd. (2012). GeoStudio Version 8.0.10 SEEP/W, Calgary, Alberta, Canada.

Huang, Y. B., G. Fipps, S. J. Maas, and R. S. Fletcher (2010), AIRBORNE REMOTE SENSING FOR DETECTION OF IRRIGATION CANAL LEAKAGE, Irrigation and Drainage, 59(5), 524-534, doi:10.1002/ird.511.

International Atomic Energy Agency (IAEA) (2008). Field Estimation of Soil Water Content – A Practical Guide to Methods, Instrumentation and Sensor Technology.

Jabro J.D., Leib, B.G., and Jabro A.D. (2005). Estimating Soil Water Content Using Site-Specific Calibration of Capacitance Measurements from Sentek Enviroscan Systems. Applied Engineering in Agriculture, 21(3): 393-399.

Jones, C. E., and R. G. Blom (2014), Bayou Corne, Louisiana, sinkhole: Precursory deformation measured by radar interferometry, Geology, 42(2), 111-114, doi:10.1130/g34972.1.

Kim, Seung-Bum and Eni G. Njoku. (2010). "Soil Moisture Retrieval Using Data Cube Representation of Radar Scattering."

Kim, Seung-Bum et al. (2011). "Soil moisture retrieval over low-vegetation surfaces using time-series radar observations and a lookup table representation of forward scattering." 2011 IEEE International Geoscience and Remote Sensing Symposium: 146-149.

Kim, Seung-Bum et al. (2012). "Soil Moisture Retrieval Using Time-Series Radar Observations Over Bare Surfaces." IEEE Transactions on Geoscience and Remote Sensing 50: 1853-1863.

Kim, Seung-Bum et al. (2014). "Models of L-Band Radar Backscattering Coefficients Over Global Terrain for Soil Moisture Retrieval." IEEE Transactions on Geoscience and Remote Sensing 52: 1381-1396.

Kim, Seung-Bum et al. (2016a). "Detection of Inland Open Water Surfaces Using Dual Polarization L-Band Radar for the Soil Moisture Active Passive Mission." IEEE Transactions on Geoscience and Remote Sensing 54: 3388-3399.

Kim, Seung-Bum et al. (2016b). "Soil Moisture Active Passive (SMAP) Algorithm Theoretical Basis Document SMAP L2 & L3 Radar Soil Moisture (Active) Data Products."

Kim, S. B., et al. (2017a), Surface soil moisture retrieval using the L-band synthetic aperture radar onboard the Soil Moisture Active Passive (SMAP) satellite and evaluation at core validation sites, IEEE Transactions on Geoscience and Remote Sensing, 55(4), 1897 - 1914.

Kim, S. B., M. Arii, and T. J. Jackson (2017b), Modeling L-band synthetic aperture radar observations through dielectric changes in soil moisture and vegetation over shrublands, Ieee Journal of Selected Topics in Applied Earth Observations and Remote Sensing, 10.1109/JSTARS.2017.2741497.

Kim, S. B., M. Moghaddam, L. Tsang, M. Burgin, X. Xu, and E. G. Njoku (2014), Models of L-band radar backscattering coefficients over the global terrain for soil moisture retrieval, IEEE Transactions on Geoscience and Remote Sensing, 52(2), 1381-1396.

Liao, T. H., S. B. Kim, A. Handwerger, E. J. Fielding, M. C. Cosh, and W. S. Schultz (2020), High Resolution Soil Moisture Maps Over Landslide Regions in Northern California Grassland, IEEE Journal of Selected Topics in Applied Earth Observations and Remote Sensing, submitted.

Madsen, S. N., and H. A. Zebker (1998), Imaging Radar Interferometry, in Principles and Applications of Imaging Radar, Manual of Remote Sensing, edited, pp. 359-380, Wiley.

Magagi, Ramata et al. (2013). "Canadian Experiment for Soil Moisture in 2010 (CanEx-SM10): Overview and Preliminary Results." IEEE Transactions on Geoscience and Remote Sensing51: 347-363.

Mancini, F.; Grassi, F.; Cenni, N., (2021), A Workflow Based on SNAP–StaMPS Open-Source Tools and GNSS Data for PSI-Based Ground Deformation Using Dual-Orbit Sentinel-1 Data: Accuracy Assessment with Error Propagation Analysis. Remote Sens., 13, 753.

Matsuoka, M. and Yamazaki, F. (2000). Use of Interferometric satellite SAR for earthquake damage detection. Proceedings of the 6th International Conference on Seismic Zonation: 103-108. EERI.

McNairn, H. et al. (2015). "The Soil Moisture Active Passive Validation Experiment 2012 (SMAPVEX12): Prelaunch Calibration and Validation of the SMAP Soil Moisture Algorithms." IEEE Transactions on Geoscience and Remote Sensing 53: 2784-2801.

Narvekar, Parag S. et al. (2015). "Soil Moisture Retrieval Using L-Band Radar Observations." IEEE Transactions on Geoscience and Remote Sensing 53: 3492-3506.

Naranjo, R.C. (2017). Knowing requires data. Groundwater 55, No. 5, 674–677.

Naranjo, R.C. (2019). Methods for installation, removal, and downloading data from the temperature profiling probe (TROD): U.S. Geological Survey Open-File Report 2019–1066, 14 p., https://doi.org/10.3133/ofr20191066.ISSN: 2331-1258.

Naranjo, R.C., and Smith, D.W. (2016). Quantifying seepage using heat as a tracer in selected irrigation canals, Walker River Basin, Nevada, 2012 and 2013: U.S. Geological Survey Scientific Investigations Report 2016-5133, 169 p., http://dx.doi.org/10.3133/sir20165133.

Naranjo, R. C., and Turcotte, R. (2015). A new temperature profiling probe for investigating groundwater-surface water interaction, Water Resour. Res., 51, 7790–7797, doi:10.1002/2015WR017574.

Narvekar, P.S., Entekhabi, D., Kim, S., and Njoku, E.G. (2013). A robust algorithm for soil moisture retrieval from the soil Moisture Active Passive mission radar observations. 2013 IEEE International Geoscience and Remote Sensing Symposium - IGARSS, 45-48.

Njoku, E. G., and D. Entekhabi (1996), Passive microwave remote sensing of soil moisture, Journal of Hydrology, 184, 101-129.

Quegan, S., T. Le Toan, J. J. Yu, F. Ribbes, and N. Floury (2000), Multitemporal ERS SAR analysis applied to forest mapping, Ieee Transactions on Geoscience and Remote Sensing, 38(2), 741-753, doi:10.1109/36.842003.

Ouellette, J. D. et al. (2017). "A Time-Series Approach to Estimating Soil Moisture From Vegetated Surfaces Using L-Band Radar Backscatter." IEEE Transactions on Geoscience and Remote Sensing 55: 3186-3193.

Ouellette, J.D., Johnson, J.T., Balenzano, A., Mattia, F., Satalino, G., Kim, S., Dunbar, R.S., Colliander, A., Cosh, M.H., Caldwell, T.G., Walker, J.P., & Berg, A.A. (2017). A Time-Series Approach to Estimating Soil Moisture From Vegetated Surfaces Using L-Band Radar Backscatter. IEEE Transactions on Geoscience and Remote Sensing, 55, 3186-3193.

Piles, Maria et al. (2009) "A Change Detection Algorithm for Retrieving High-Resolution Soil Moisture From SMAP Radar and Radiometer Observations." IEEE Transactions on Geoscience and Remote Sensing 47: 4125-4131.

Simonds, J., (1996). The Newlands Project: Bureau of Reclama¬tion Report, 39 p., http://www.usbr.gov/projects//ImageServer?imgName=Doc_1305124117489.pdf.

Tabatabaeenejad, A., R. H. Chen, M. S. Burgin, X. Y. Duan, R. H. Cuenca, M. H. Cosh, R. L. Scott, and M. Moghaddam (2020), Assessment and Validation of AirMOSS P-Band Root-Zone Soil Moisture Products, Ieee Transactions on Geoscience and Remote Sensing, 58(9), 6181-6196, doi:10.1109/tgrs.2020.2974976.

Wang, S. G. et al. (2011). "Estimation of surface soil moisture and roughness from multi-angular ASAR imagery in the Watershed Allied Telemetry Experimental Research (WATER)."

Waterloo Hydrogeologic, Inc. (2016). Visual MODFLOW v.5.0, Integrated Conceptual and Numerical Groundwater Modeling Software, Schlumberger Water Services, Waterloo Hydrogeologic Division, Kitchener, Ontario, Canada.

Yamazaki, F. (2003). Remote Sensing Technology for Earthquake Damage Detection. Institute of Industrial Science, University of Tokyo, Tokyo, Japan. Earthquake Disaster Mitigation Research Center, NIED, Kobe, Hyogo, Japan.

Yunjun, Z., Fattahi, H., and Amelung, F. (2019), Small baseline InSAR time series analysis: Unwrapping error correction and noise reduction, Computers & Geosciences, 133, 104331, doi:10.1016/j.cageo.2019.104331.

Zhu, X. L., J. Chen, F. Gao, X. H. Chen, and J. G. Masek (2010), An enhanced spatial and temporal adaptive reflectance fusion model for complex heterogeneous regions, Remote Sensing of Environment, 114(11), 2610-2623, doi:10.1016/j.rse.2010.05.032.